Estimation of Heating-Up Effecting in the Yellow River Basin Based on MODIS Data

Ziwu Pan
Henan University
Jun Zhu
Henan University
Fen Qin (qinfun@126.com)
Henan University

Research Article

Keywords: Modis, Air temperature, GWR method, Heating-up effect

Posted Date: May 17th, 2021

DOI: https://doi.org/10.21203/rs.3.rs-515924/v1

Estimation of heating-up effecting in the Yellow River Basin based on MODIS data

ZiwuPan[a,b],**Jun Zhu**[a,b], **Fen Qin**[a,b,*]

a:College of Environment and Planning, Henan University,Kaifeng, China;wugemicheal@163.com (Z.P.); ZhuJun@126.com(Z.J.);

b:Laboratory of Geospatial Technology for the Middle and Lower Yellow River Regions, Henan University, Kaifeng, China

*Correspondence: qinfun@126.com; Tel.: +86-135-0378-5302

Abstract: Using MODIS land surface temperature data, air temperature data and elevation data from 2000 to 2015 in the Yellow River Basin. The GWR analysis method with high accuracy was chosen to establish the regression model of plateau air temperature, land surface temperature and altitude. In the 12-month GWR regression model, the determination coefficient (Adjusted $R^{2)}$ was above 0.95 or more (0.959-0.980) and the root-mean-square error (RMSE)was between 0.740 and 1.029°C. Depending on the model, the air temperature of the Yellow River Basin is estimated and the accuracy is verified. On this basis, the average monthly air temperature in the basin is converted to altitudes of 4500m and 5000m, and the heating-up effects of various shapes in the basin are compared and discussed. The results show that: (1) Using the GWR method, combined with the observation data of the ground station, the accuracy of the air temperature estimation in the Yellow River Basin can be increased to 0.740°C; (2) According to the estimated annual variation of the spatial distribution of the 12-month average temperature, in the upper of the Tibet Plateau, the Huangshui Valley and the Gannan Plateau have lower annual air temperatures and less spatial distribution. While the air temperature in the northeast of the upstream Inner Mongolia plateau was higher, which was related to the rapid drying temperature rise near the desert. The change of mean monthly temperature in the middle and lower reaches is relatively high and the change is small, which is closely linked to the fact that it is located in the low-elevation area of the basin plain and has perennial light and heat.(3) The heating-up effect in the Yellow River Basin is outstanding. It is preliminaries estimated that at the same altitude, the Tibet Plateau is about 1.5~8°C higher than the Loess Plateau, and about 6~13°C higher than the North China Plain.

Keywords: Modis; Air temperature ; GWR method; Heating-up effect

1 Introduction

Heating-up effect has long been the focus of scholars, referring to the thermal effects of the bulging mountain, leading to the temperature-dependent vertical boundary of the mountain (timberline, snow line) in the inland giant mountain or mountain center than the

peripheral area or coastal. The phenomenon of high regional distribution is the main factor affecting the distribution of altitudinal zones on a large scale, and is an important mechanism for the spatial pattern and dynamic change of the geographic surface system[1-4]. The thermal effect of the mountain produces a temperature space pattern that the internal temperature of the mountain is higher than the outside at the same altitude, which the essence is that the mountain or plateau uplift has increased the temperature effect on the surrounding atmosphere [5-7]. The Yellow River Basin has a large geographical span and flows through most of northwest and north China, which has a major impact on the Asian climate. The Yellow River Basin is bounded by the Bayan Kala Mountain in the west, the Yinshan Mountain in the north, the Qinling Mountains in the south, and the Bohai Sea in the east. Topography within the basin is with large differences that is high in the west and low in the east, while it has crossed the three-level ladder of China from west to east. The terrain in the area is complex and diverse, but the stations across the meteorological observatory are very rare as well as the temperature data is scarce. So it is difficult to conduct in-depth and quantitative research on the temperature heating-up effect [8-10]. The air temperature in the Yellow River Basin is mainly obtained through a series of statistical analyses and spatial interpolation basing on the observation data of discrete meteorological stations. For example, Pan Pan et al. used the statistical analysis method based on observation data from 142 stations in the Yellow River Basin to study the interdecadal variations of the Yellow River Basin in the past 50 years, revealing the temporal and spatial distribution as well as variation characteristics of the Yellow River basin [11]; Huang Xing et al. used the data from 52 stations in the Inner Mongolia section of the Yellow River Basin from 1951 to 2012 to study the air temperature variability and warming stagnation of the Yellow River Basin in the past 60 years, while studied the trend of air temperature variation in the typical region of the Yellow River Basin [12]; These studies all focused on the use of statistical methods to study the interannual variation of temperature in the Yellow River Basin, which the results can reflect the temporal variation of temperature and the overall variation of the region to a certain extent, but it cannot accurately reflect the detailed spatial distribution of air temperature [13-15].

At present, the most common way to get the air temperature of a certain spatial location is to obtain the data from the existing meteorological stations [16]. In the Yellow River Basin, on the one hand, due to the scarcity of meteorological stations, on the other hand, because the plateau types and plains are interlaced in the basin and the types of landforms are diverse, the spatial position of these stations cannot fully reflect the spatial variability of air temperature[17,18]. Yao Yonghui et al. conducted a detailed discussion on the variation characteristics and regional differences of annual average temperature and precipitation from 1960 to 2008 in the Hengduan Mountains, with selecting the 27 weather stations with the longest measured data sequence in the region. It is proposed that the air temperature in the Hengduan Mountains showed a statistically warming trend in the past 50 years[19]. In order to obtain more accurate interpolation results, Hwang et al. (2005) generated high-precision global temperature and precipitation interpolation by of longitude, latitude and altitude as variables based on global 1950-2000 meteorological observation data and 90m resolution SRTM topographic data, which , however, because the samples are very rare, there is a large uncertainty in the data in the mountains[20]. Factors affecting temperature such as soil temperature and humidity, vegetation cover, mountain heating-up effect, slope topographic

conditions, precipitation, etc. [21], it is difficult to obtain detailed data at the same scale, which has become the bottleneck of air temperature space interpolation. [22-24].

With the development of thermal infrared remote sensing technology, it provides a more efficient and effective way to obtain spatial data of air temperature [25]. Han Fang et al. combined MOD11C3 land surface temperature products and the measured temperature data from 144 meteorological stations on the ground to estimate the air temperature difference at the same height inside and outside the Tibet Plateau. It shows that the air temperature difference between the inner and outer parts of the data point is closely related to the height of the local base surface.While height of the base surface increases by 100 m,the air temperature difference increases by about 0.051°C [26, 27].Hongmei Zhang developed a method for estimating the daily average near-surface air temperature by using estimating daily maximum and minimum air temperaturesfrom time series observed with Moderate Resolution Imaging Spectroradiometer (MODIS) and Atmospheric Infrared Sounder (AIRS). The advantage is that it can obtain reasonable near-surface air temperature data from remote sensing data, with mean absolute error (MAE) and root-mean-square error (RMSE) of 1.2°C and 1.6 °C respectively[14]. Didari et al. used a stepwise linear model to estimate the minimum LSAT5cm for the period 2003-2011, by using land surface temperature (LST) data and normalized differential vegetation index(NDVI) from MODISAqua and Terra satellites, as well as geometric temperature and elevation information. The results show that the accuracy of winter estimation is lower than other seasons (RMSD=3.55°C), and the errors in summer and winter are greater than the rest of the season [28]. Zhang, F. et al. estimated the ground observation of four glaciers on the Qinghai-Tibet Plateau. The daily temperature indicates that the RGS model based on MODIS nighttime data is significantly better than the model based on MODIS daytime data in estimating the daily average, minimum and maximum temperatures, which is effective to limit the MODIS daily four observations data to non-cloudy[29]. YulinCai et al. connected the daily maximum surface temperature (Tamax), surface temperature, and five major land cover types in the growing and non-growing stages of the middle and lower reaches of the Yangtze River by using the medium-resolution imaging spectrometer surface temperature (LST) product. Statistical models were developed to show that the modeling performance of the Tamax-LST relationship is highly dependent on land cover and seasonal variation [30]. Bo-Hui Tang et al. compare the use of the medium resolution imaging spectrometer product MOD11_L2/MYD11_L2 and in situ LST in the field of the Hailar field in northeastern China, showed that the LST retrieval accuracy can be improved by 0.4K by reparameterizing the GSW coefficients using an ATI profile from a thermodynamic initial guess to retrieve a cloudless database [31]. Based on MODIS land surface temperature data, 137 meteorological observatory data and ASTERGDEM data, Yao Yonghui established a regression model of plateau air temperature, land surface temperature and altitude, estimated the air temperature of the Tibet Plateau, and made comparative analysis of the heating-up effect inside the plateau relative to the peripheral areas[32]. This study shows that using MODIS land surface temperature can accurately estimate mountain air temperature. The air temperature estimation based on MODIS land surface temperature also shows that the land surface temperature obtained by thermal infrared remote sensing has a good linear relationship with the air temperature [33-36]. The air temperature can be estimated accurately by land surface temperature (RMSE is basically around 1~3°C), which

can get more detailed information on air temperature and space changes [37-40].

Studying the heating-up effect of the mountain and estimating the difference between the mountains at the same altitude is the key to quantifying the mountain effect. The LST data provided by the MODIS sensor has medium spatial and temporal resolution, which has been widely used in station temperature estimation for sparse mountainous areas. Although many studies have estimated the air temperature of different regional types, however, the accuracy needs to be improved. Based on Modis data and air temperature data, this paper estimates the air temperature of the Yellow River Basin with high precision and obtains the air temperature difference between different terrain heights in the region, thus realizing the quantification of the mountain effect in the Yellow River Basin. The research purposes of this paper are as follows: (1) To analyze the time series changes of air temperature and land surface temperature, and to reflect the difference between air temperature and land surface temperature by detecting and characterizing Breaks For Additive Seasonal and Trend (BFAST). (2) Using the geo-weighted regression analysis method based on spatial heterogeneity theory, estimate the average monthly air temperature of the Yellow River Basin with the long-term sequence of MODIS land surface temperature data combining with air temperature data and DEM data. (3) Taking the special topography of the Yellow River Basin, draw strips across the Tibet Plateau, the Loess Plateau and the North China Plain, focusing on the air temperature distribution and heating-up effect in the Yellow River Basin.

2 Study area and data

2.1 Study area

The Yellow River Basin traverses East and West China, most of which are situated in the northwest of China (Fig.1). Located between 95°53′～119°05′ E and 32°10′～41°50′ N, it is 1900km long from east to west and 1100km wide from north to south, with a drainage area of 795,000 square kilometers. The Yellow River Basin has a vast territory and a huge difference in topography. The drainage area is high in the west and low in the east. The average elevation of the western Heyuan area is above 4000m. It consists of a series of lofty mountains, with snow all over the year and glacial landforms. The elevation of the central area is between 1000 and 2000m, which is the loess landform with serious soil erosion. Not more than 50 meters are mainly composed of the alluvial plains of the Yellow River, where the river overhangs the ground, posing a great flood threat.The distribution of meteorological stations in the study area is uneven, and the detailed data of meteorological elements such as temperature and precipitation are scarce. The estimation of temperature by means of thermal infrared remote sensing can provide an important means for climate research in this region.

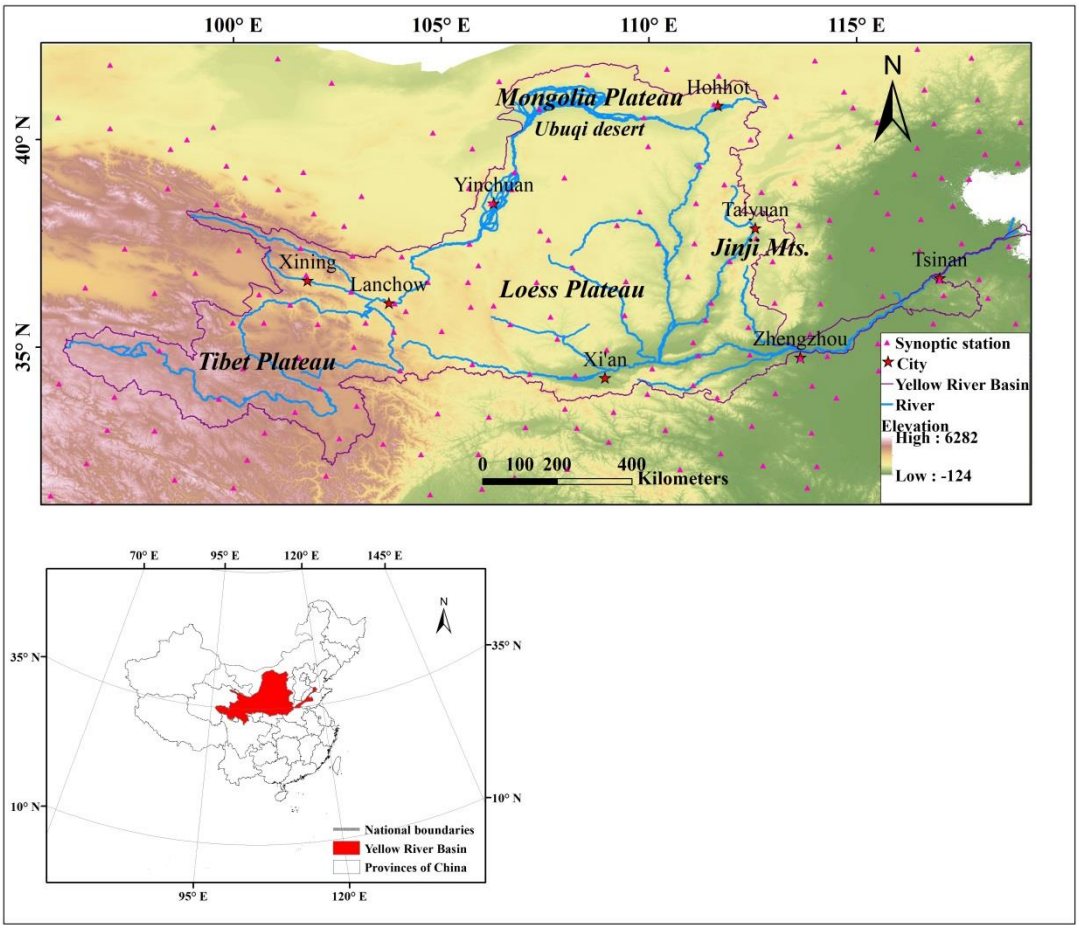

Fig.1 Study area and weather station distribution map

2.2 Data

Land Surface Temperature data are MODIS Terra/Aqua global monthly mean surface temperature/emissivity data with a spatial resolution of 1 km, from 2000 to 2015. The data product is Terra/Aqua Monthly Land Surface Temperature & Emissivity (MODLT1T), and the data is from the International Scientific & Technical Data Mirror Site (Computer Network Information Center, Chinese Academy of Sciences.). Owing to the influence of clouds, there are some missing values in these MODIS surface temperature data, mainly distributed in the middle of the Loess Plateau. We replace these missing values with the nearest neighbor method with elevation.

The air temperature data used in this paper are the average monthly temperature data from 2000 to 2015, taken from the China Meteorological Information Center China Land Climate Data Monthly Value Data Set (http://cdc.cma.gov.cn/index.jsp). After strict quality control and screening, the data using the 1km resolution topographic map DEM of the Yellow River Basin as a covariance, using the AUSPLIN software spline method (TPS, Thin Plate Spline) for spatial interpolation, the generated ground horizontal resolution of 1km × 1km of monthly grid data.

ASTERGDEM data is downloaded from http://www.gdem.aster.ersdac.or.jp. The spatial resolution is 30 m. In order to estimate the temperature together with the MODIS land surface

temperature data, re-sampling is performed in a grid unit of 1 km x 1 km.

3 Method

Average monthly land surface temperature data of MODIS Terra/Aqua 2000-2015 are compared with the average monthly air temperature data of meteorological data. The average monthly land surface temperature data of day and night in Terra surface temperature data set are averaged to obtain the monthly mean surface temperature (Ts) of the Yellow River Basin from 2000 to 2015 and a corresponding database is established; on this basis, the following analysis is performed:

(1) ① BFAST algorithm

This method [41] decomposes the integrated time series into three parts: trend, seasonality and residual, and detects and characterizes the sudden changes in the trend and seasonal parts according to a certain method. Suppose an additive decomposition model can iterate to a piecewise linear model that matches the trend and seasonality. The algorithmic form of the model is:

$$Y_t = T_t + S_t + e_t,\ t = 1, \cdots, n \qquad (1)$$

where Y_t is the value observed at time t; T_t is the trend component; all is the seasonal component. e_t is the residual part, that is, the variable component outside the seasonality and the trend. Suppose the change of T_t is piecewise linear and there are $t_1^*, \cdots, t_m^*$, and define t_0^*:

$$T_t = \alpha_j + \beta_j t \qquad (2)$$

where the range of t is $t_{j-1}^* < t \leqq t_j^*$, and j=1,⋯,m; α_j and β_j; are the intercept and slope of the continuous linear model, respectively, which can be obtained from the magnitude and direction of the sudden change. It is the slope of the gradual change between the detection breakpoints. The change size of each mutation point is the difference of T_t between t_{j-1}^* and t_j^*.

The seasonal trend can be expressed as:

$$S_t = \sum_{i=1}^{s-1} \gamma_{i,j} \left(d_{t,i} - d_{t,0} \right) \qquad (3)$$

where s is the seasonal duration (such as the number of observations per year); $\gamma_{i,j}$ is the influence factor of the i-th period. When time t is the i-th observation, $d_{t,i}$=1, otherwise 0. Therefore, when t is the seasonal zero period, $d_{t,i} - d_{t,0}$= -1. When t is other seasonal period, $d_{t,i} - d_{t,0}$ = 1. $d_{t,i}$ usually considered as seasonal dummy variable, it has two available values of 0 and 1 to explain the seasonal period in the regression model.

② Iterative Algorithms

Before fitting the piecewise linear model and estimating the mutation point, first test whether any mutation point appears in the time series. The ordinary least squares OLS (ordinary least squares) residual based on the moving sum (moving sum) test is used to test whether there are one or more mutation points. If a significant change is tested (P<0.05), Bai and Perron's method is used to estimate the mutation points, and the number of mutation points, as well as the time and confidence interval of the mutation points, are determined according to the Bayesian information criterion.

The iterative algorithm starts with the STL method to estimate $\hat{S}_t$, where $\hat{S}_t$ is estimated from the mean of all seasonal subsequences. After that, the iterative algorithm follows the following 4 steps:

1) If the OLS-MOSUM test shows that there are mutation points in the trend component,

the number and location (time) information of these mutation points ($t_1^*,\cdots,t_m^*$) can be estimated from the corrected seasonal data to get $Yt-\hat{S}_t$.

2) The trend coefficients α_j,β_j, in the interval j=1,$\cdots$,m are calculated by the robust regression equation (2) based on the M estimation method. The trend estimate is:

$$\hat{T}_t = \hat{\alpha}_j + \hat{\beta}_j t, t = t_{j-1}^* + 1, \ldots., t_j^* \qquad (4)$$

3) If the OLS-MOSUM test shows that the mutation point appears in the seasonal component, the number of seasonal mutation points ($t_1^{\#},\ldots.,t_p^{\#}$) and the location (time) can be estimated from the trend data $Yt-\hat{T}_t$.

4) The seasonal coefficient $\gamma_{i,j}$(i=1,$\cdots$,s-1; j=1,$\cdots$, m) can be calculated from the regression equation based on the M estimation method. The seasonal estimation formula is:

$$\hat{S}_t = \sum_{i=1}^{s-1} \hat{\gamma}_{i,j}\left(d_{t,i} - d_{t,0}\right), t = t_{j-1}^{\#} + 1, \ldots., t_j^{\#} \qquad (5)$$

(2)The GWR method is used to estimate the regression equation of air temperature and MODIS land surface temperature and altitude at each given location in the study area (formula (5)), and generate the land surface temperature coefficient surface, the altitude coefficient surface and the constant term coefficient surface. Establish a GWR regression model for temperature estimation.

$$T\alpha_i(u) = \beta_{0i}(u) + \beta_{1i}(u)Ts_i(u) + \beta_{2i}(u)h_i(u) \qquad (5)$$

Where $T\alpha$ represents air temperature; Ts represents MODIS land surface temperature; h represents the altitude; u represents a certain spatial position; i = 1, ...n, represents the number of spatial positions; β is the corresponding coefficient term.Gaussian and bi-square kernel functions are two common kernel types for GWR.The Gaussian kernel weights continuously and gradually decrease from the center of the kernel; however, theweights never reach zero. The adaptive Gaussian kernelfunction is as follows:

$$\omega_{ij} = \exp\left(-\left(\frac{d_{ij}}{b}\right)^2\right) \qquad (6)$$

Where $d_{ij}$is the distance between the sites and $b$is anadaptive bandwidth size that is defined as the nearestneighbour distance.

The bi-square kernel function has a clear-cut rangewhere the weighting is non-zero. In this study, the adaptivebi-square kernel function was used to describe the spatialdependence of the data:

$$w_{ij} = \begin{cases} \left[1 - \left(\frac{d_{ij}}{b}\right)^2\right]^2 & d_{ij} \le b \\ 0 & d_{ij} > b \end{cases} \qquad (7)$$

The selection of an appropriate bandwidth requires careand in some instances may benefit from a measure of howwell the model fits the data. An interval search was used todetermine the optimal bandwidth of the adaptive bi-squarekernel function.

(3)The high-precision GWR model is used to estimate the average monthly air temperature of the basin for 12 months. In this paper, the air temperature is converted into sea level temperature for related research [42], and the average monthly air temperature of the plateau is converted to the average altitude of the Tibetan Plateau within the basin, which

was 4,500m and 5000m respectively, so as to compare the differences of geomorphic units within the basin:

$$Ta_h = Ta + (elevation - h) \times 0.006 \quad (8)$$

Where h is the specified altitude, in this paper 4,500 m and 5000 m; Tah and Ta are the air temperature and the actual temperature at a specified altitude, h, respectively. Vertical decline rate of temperature still uses the average vertical temperature decline rate of 0.006°C/m.

4 Results and discussion

4.1 Data analysis results

Through the time series analysis of MODIS land surface temperature and air temperature data in different months of the study area, the average monthly temperature of MODIS land surface temperature is generally consistent with the air temperature change regularity, and the root mean square error of each month is statistically analyzed (Table 1). The RMSE of48%~82% is lower than 4°C, and the RMSE of about 2%~19% is higher than 6°C. The location of the root mean square error is mainly concentrated in the upper reaches of the Tibet Plateau in the upper reaches of the Yellow River Basin, the eastern and western parts of the Loess Plateau and in the middle of the Inner Mongolia Plateau, there are mountains such as Qilian Mountain, Helan Mountain, Yin Mountain and Taihang Mountain. The reasons for this analysis are: (1) The complex and diverse topographical conditions of the Yellow River Basin, such as altitude and surface roughness and undulation, will have a strong influence on the temperature. (2) The impact of vegetation covers during the growing season. Existing research has also shown that different types of ecosystems and land cover have a greater impact on temperature. During the growing season, different types of vegetation return to green and grow, which has a greater impact on surface temperature [43-45], which may be the main reason for the significant difference between Ts and Ta in the growth period of the Yellow River Basin. (3) The complex geography, climate, ecology and natural environment in the basin will have a certain degree of influence on the inversion accuracy of the surface temperature, thus increasing the error of temperature estimation accuracy.

Table 1 The result of RMSE between Ta and Ts

Month	Extent(°C)	Less than 2 °C(%)	2 °C ~ 4 °C (%)	4 °C ~ 6 °C (%)	Greater than6 °C(%)
Jan.	0.433-12.139	44.047	44.431	9.401	2.121
Feb.	0.507-11.382	25.172	53.005	18.071	3.752
Mar.	0.553-12.501	17.534	37.321	33.953	11.182
Apr.	0.451-14.704	19.015	31.212	35.220	14.553
May	0.628-14.220	19.354	29.562	34.431	16.653
Jun.	0.404-13.188	23.856	30.640	28.102	17.402
Jul.	0.425-13.511	31.973	27.462	22.334	18.231
Aug.	0.431-13.851	34.047	27.310	21.981	16.662
Sep.	0.396-13.431	29.402	34.153	25.921	10.524
Oct.	0.402-13.051	20.313	48.754	24.962	5.971
Nov.	0.464-14.750	32.024	50.123	14.272	3.581

4.2 GWR analysis

Although the air temperature in the basin has a linear relationship with the land surface temperature, the air temperature is still spatially different. Therefore, the altitude factor is introduced into the GWR regression analysis method to estimate the air temperature. The GWR regression analysis results (Table 2) show that, from the estimation, the 12-month decision coefficient (Adjusted R^2) is higher than 0.95 (0.959-0.980), and the RMSE of each month is between 0.740 and 1.029°C, the accuracy is higher.

Table 2 Results of GWR analysis for each month

Statistical Index	Jan.	Feb.	Mar.	Apr.	May	Jun.	Jul.	Aug.	Sep.	Oct.	Nov.	Dec.
Sigma	0.811	0.915	0.992	1.089	1.132	1.073	1.012	0.988	0.900	0.829	0.876	0.990
R^2	0.981	0.965	0.960	0.961	0.970	0.980	0.981	0.979	0.977	0.976	0.971	0.971
Adjusted R^2	0.980	0.964	0.959	0.959	0.969	0.979	0.980	0.978	0.976	0.975	0.970	0.970
RMSE(°C)	0.760	0.940	0.967	1.000	1.029	0.989	0.980	0.915	0.777	0.740	0.899	1.015

306 4.3 Air Temperature estimation and heating-up effect analysis

307 4.3.1 Air Temperature estimation and precision evaluation

308 Using the GWR method to generate the land surface temperature coefficient and air
309 temperature surface coefficient , the surface of the altitude coefficient and the surface of the
310 constant term coefficient, and establish a GWR regression model to estimate the monthly
311 mean air temperature of the Yellow River Basin. To further evaluate the accuracy of the model
312 estimates, 225 meteorological stations were used as verification points in the study area. The
313 results of the error verification show that (Table 3), except for the maximum error from April
314 to August, which is 1.043-1.109°C, the estimation error of extra months is less than 1°C. The
315 verification results show that the estimation accuracy of the GWR method can be controlled
316 within 1.2°C. Accuracy analysis results show that the accuracy of the temperature in the
317 Yellow River Basin based on MODIS land surface temperature, meteorological data and DEM
318 is very high.
319
320 **Table 3** Site verification error

Month	Residual		Local R^2	RMSE(°C)
	Range(°C)	-1.2°C~1.2°C(%)		
Jan.	-3.194-1.328	92.445	0.003-0.867	0.631-0.804
Feb.	-2.949-3.653	82.667	0.002-0.909	0.770-0.906
Mar.	-3.057-3.964	77.778	0.001-0.945	0.831-0.983
Apr.	-2.738-4.567	74.111	0.001-0.945	0.911-1.067
May	-3.597-4.713	66.222	0.001-0.953	0.946-1.109
Jun.	-6.086-3.508	68.444	0.003-0.959	0.899-1.063
Jul.	-5.914-4.004	66.222	0.001-0.963	0.867-1.068
Aug.	-5.334-4.056	68.444	0.001-0.952	0.846-1.043
Sep.	-3.760-3.605	75.556	0.007-0.953	0.755-0.892
Oct.	-2.161-2.543	83.556	0.003-0.942	0.696-0.821
Nov.	-2.350-3.463	84.889	0.004-0.936	0.739-0.868
Dec.	-2.868-3.801	81.778	0.004-0.921	0.843-0.981

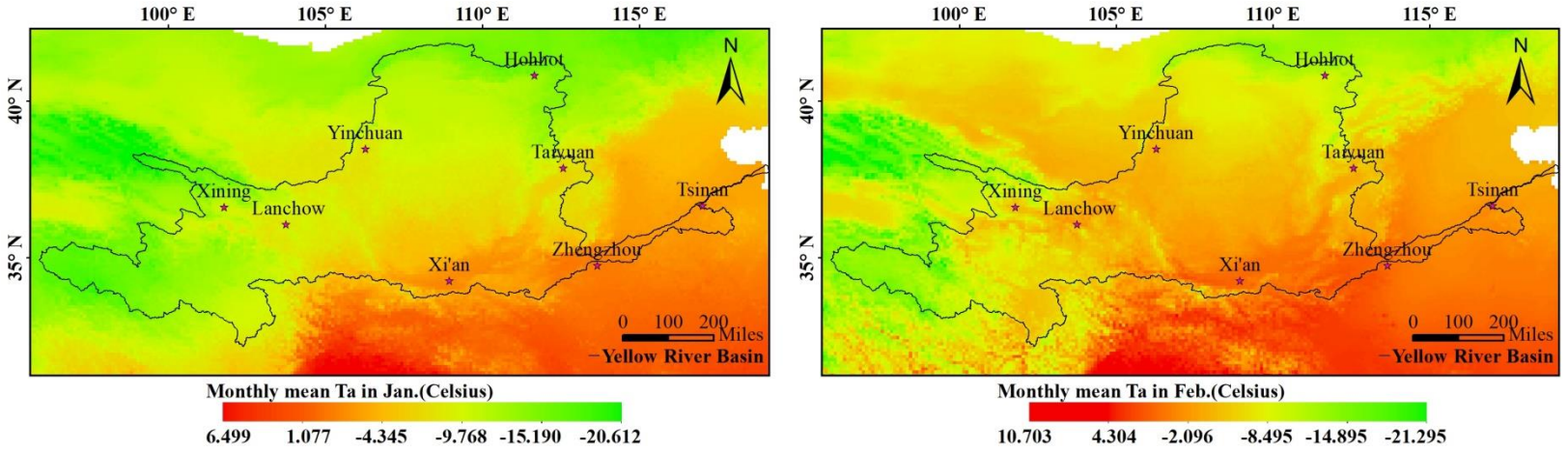

321

322

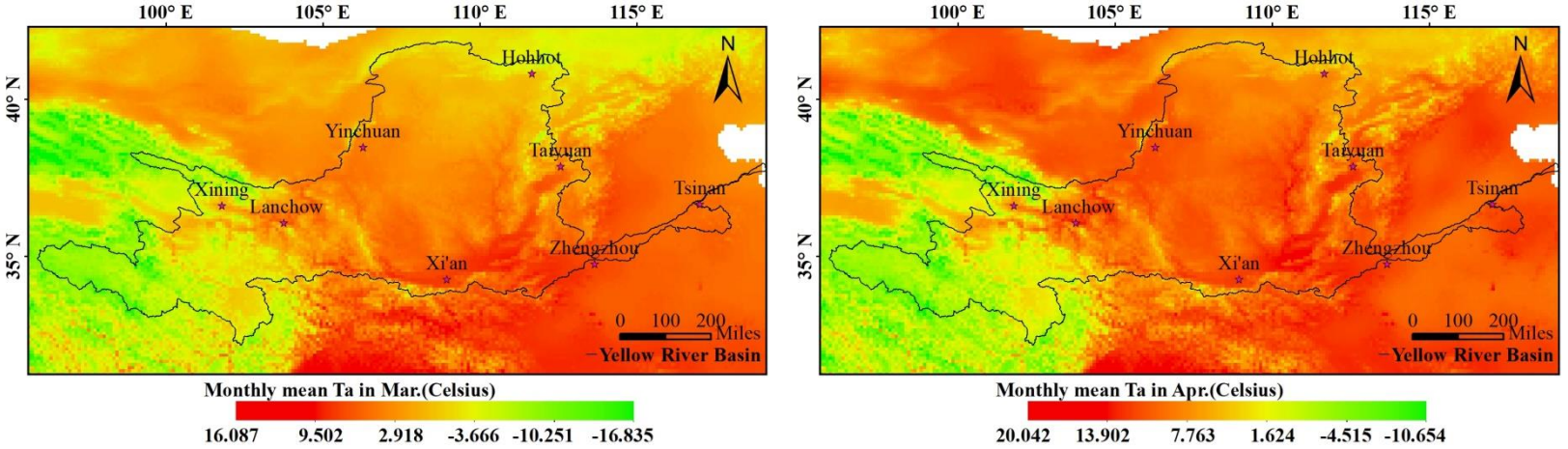

323

324

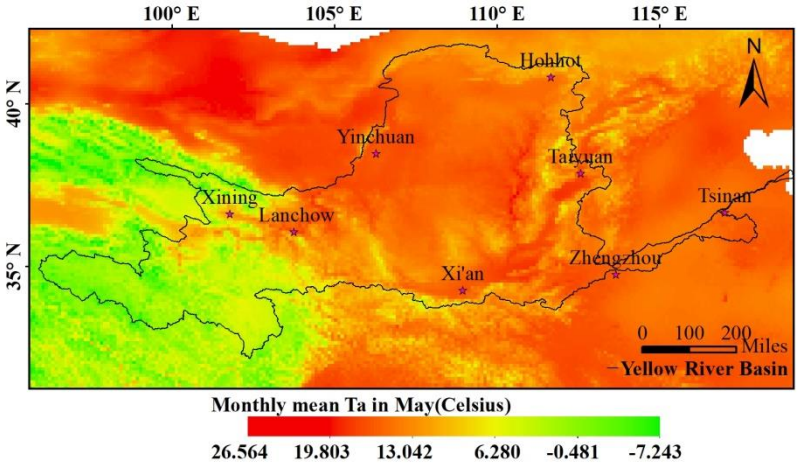
100° E
105° E
110° E
115° E
40° N
35° N
N
Hohhot
Yinchuan
Taiyuan
Xining
Lanchow
Tsinan
Zhengzhou
Xi'an
0 100 200
Miles
Yellow River Basin
Monthly mean Ta in May(Celsius)
26.564 19.803 13.042 6.280 -0.481 -7.243

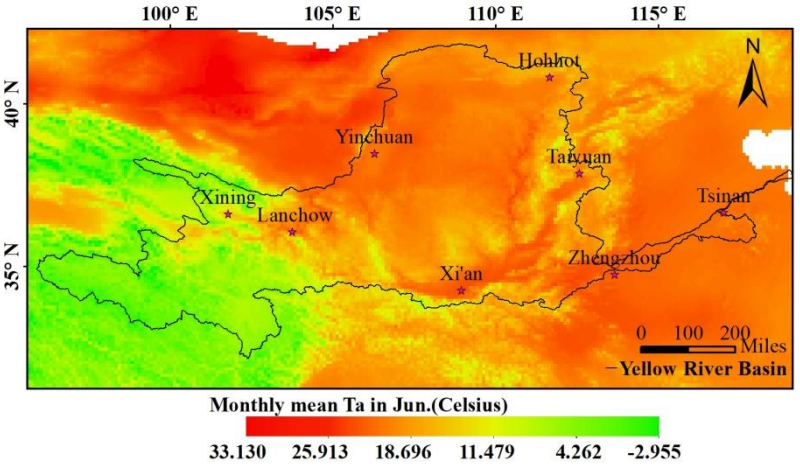
100° E
105° E
110° E
115° E
40° N
35° N
N
Hohhot
Yinchuan
Taiyuan
Xining
Lanchow
Tsinan
Zhengzhou
Xi'an
0 100 200
Miles
Yellow River Basin
Monthly mean Ta in Jun.(Celsius)
33.130 25.913 18.696 11.479 4.262 -2.955

325

326

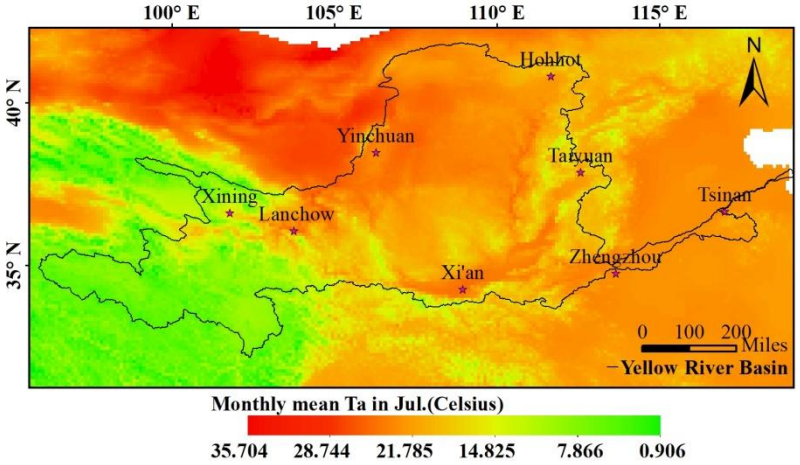
100° E
105° E
110° E
115° E
40° N
35° N
N
Hohhot
Yinchuan
Taiyuan
Xining
Lanchow
Tsinan
Zhengzhou
Xi'an
0 100 200
Miles
Yellow River Basin
Monthly mean Ta in Jul.(Celsius)
35.704 28.744 21.785 14.825 7.866 0.906

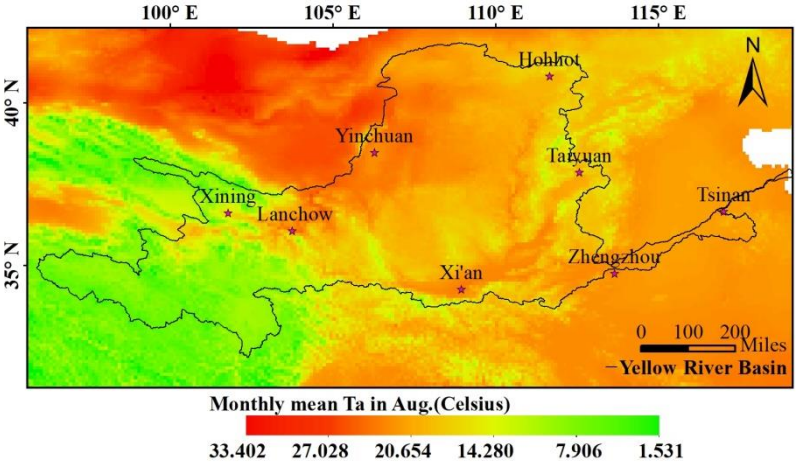
100° E
105° E
110° E
115° E
40° N
35° N
N
Hohhot
Yinchuan
Taiyuan
Xining
Lanchow
Tsinan
Zhengzhou
Xi'an
0 100 200
Miles
Yellow River Basin
Monthly mean Ta in Aug.(Celsius)
33.402 27.028 20.654 14.280 7.906 1.531

327

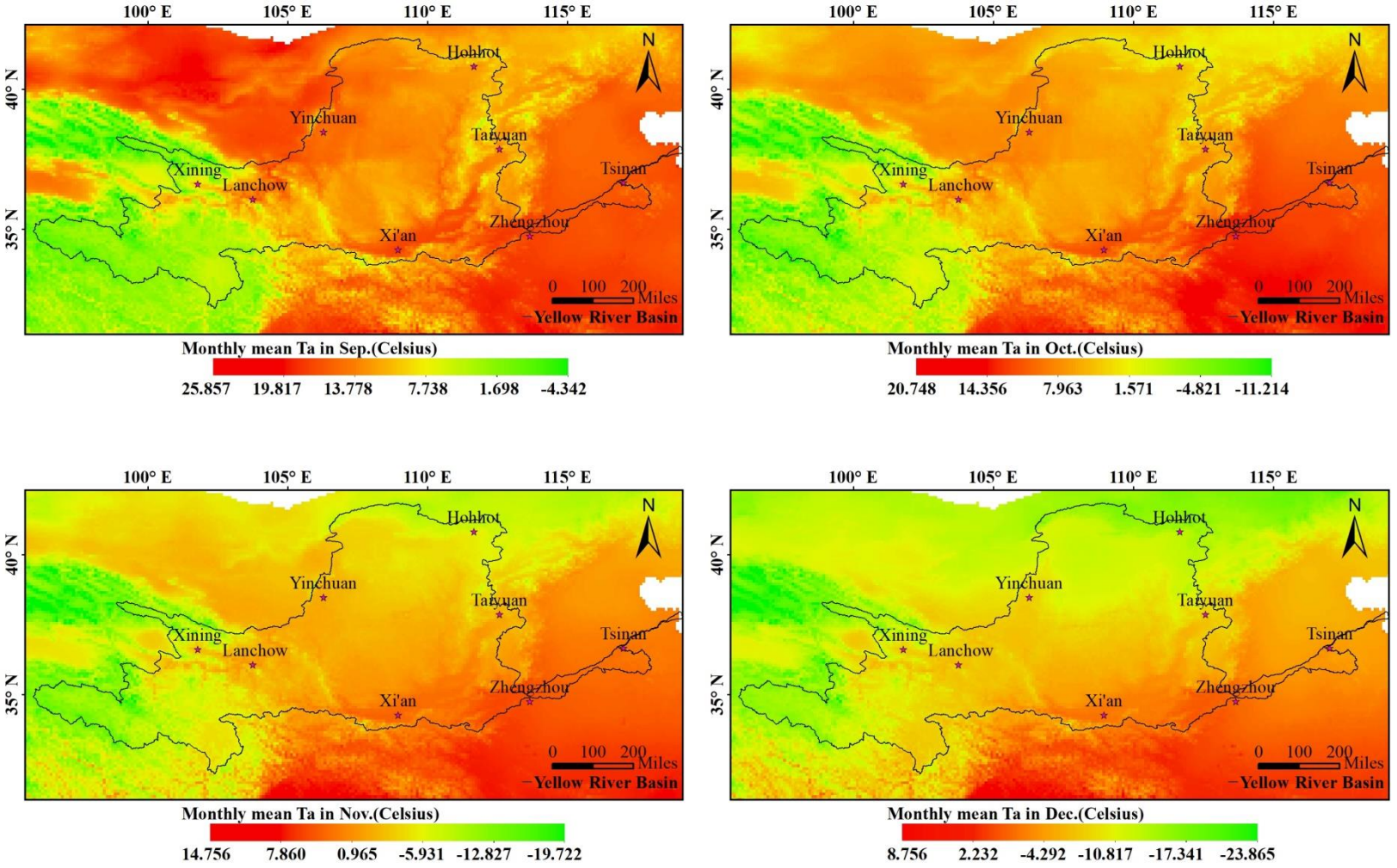

Fig.2 Spatial distribution of monthly mean Ta in the study area

4.3.2 Analysis of heating-up effect in the Yellow River basin

According to the spatial distribution of the estimated air temperature(Fig. 2), it can be seen that the air temperature range in January (the coldest month) is -20.612~6.499°C, and the air temperature range in July (the hottest month) is 0.906~35.704°C; The air temperature in each month is generally low in the west and high in the east, followed by the north-central characteristics, and the reason is that the west is located in high altitude areas such as plateaus and mountains, and the annual air temperature is low. The central and northern parts are mainly the central Long, the eastern Long of Loess Plateau and the Inner Mongolia Plateau and it has a deep inland rainfall and a dry climate; the downstream is located in the plain area and has a low latitude, and accept quantity of heat sufficient all the year round, so the temperature is high.According to the estimated annual variation of the spatial distribution of the 12-month average air temperature, in the upper of the Tibet Plateau, the Huangshui Valley and the Gannan Plateau have lower annual air temperatures and less spatial distribution.While the air temperature in the northeast of the upstream Inner Mongolia plateau was higher, especially The Wula Mountain, the YinshanNantun and the Daqingshan area are the most typical, which was related to the rapid drying temperature rise near the desert. The change of average monthly air temperature in the middle and lower reaches is relatively high and the change is small, which is closely linked to the fact that it is located in the low-elevation area of the basin plain and has perennial light and heat.

In addition, in order to further compare the spatial distribution and difference of the air temperature inside the basin, the special terrain of the Yellow River Basin is used to draw the distribution of temperature across the Tibet Plateau, the Loess Plateau and the North China Plain to focus on the study of the air temperature distribution regulation and heating-up effect in the region (Fig. 3 Fig. 4), the air temperature inside the strip has the following characteristics:

a) From May to September in the summer half year, the 10°Cisotherm is mainly distributed in height of 3000~4700m in the Tibet Plateau. The 10°C isotherm in October is mainly distributed at the height of 900~2700m in the Loess Plateau. The Tibet Plateau also has scattered distribution. In the summer half year, the 10°C isotherm has gradually increased from 3432m to the highest value of 4276m (July) since May, and then gradually decreased to the lowest value of 2002m (October); the winter half year refers to November to April of the following year. The 0°C isotherms in March and April are mainly distributed at the altitude of 3000~3900m on the Tibet Plateau. The 0°C isotherms in other months of the winter months are mainly distributed at the height of 600~3000m on the Loess Plateau and 30~600m in the North China Plain. In the winter half year, the 0°C isotherm has gradually decreased from 2933m to the lowest value of 170m (January) since November. Since then, the 0°C temperature line has gradually recovered and reached the highest value of 4338m in April. Distribution height of the isotherm in the area gradually rises from the North China Plain to the Loess Plateau to the Tibet Plateau, the lowest in the North China Plain and the highest in the Tibet Plateau. Therefore, it can be seen from the elevation of the isotherm that it gradually rises from the east to the west of the Yellow River Basin.

b) In terms of air temperature, the plateau heating-up effect is manifested in the same altitude. The air temperature of different geomorphic units in the Yellow River basin at the

same altitude is compared, and the air temperature difference of different geomorphic units at the same altitude is calculated.The average monthly air temperature was converted to the altitude of the Yellow River basin in accordance with equation (5), which was 4500m and 5000m, and the air temperature profile was made along the east-west direction(Fig. 5, Fig. 6). From the air temperature at the same altitude in the Tibet Plateau, the Loess Plateau and the North China Plain, the air temperature in the Tibet Plateau is higher than that in the Loess Plateau and North China, andthe Loess Plateau is higher than the North China Plain, regardless of the coldest month (January) or the hottest month (July). The air temperature difference from the altitude of 4500m can be seen (Table 4, Figure 7). The air temperature difference between the Loess Plateau and the North China Plain in January (the coldest month) is 3.020°C, and the air temperature difference in July (the hottest month) is 5.783°C, the annual air temperature difference is 3.020°C(January)~6.705°C(April); the temperature difference between the Tibet Plateau and the Loess Plateau in January (the coldest month) is 7.285°C, and the temperature in July (the hottest month) The difference is 3.141°C, the annual temperature difference is 1.515°C(June)~7.724°C(December); the temperature difference between the Tibet Plateau and the North China Plain in January (the coldest month) is 10.305°C, July (the hottest month) The temperature difference is 8.924°C, and the annual temperature difference is 6.333°C(June)~12.355°C(February). It can be seen from the above analysis that at the same altitude, the Loess Plateau is higher than the North China Plain, and the temperature of the Tibet Plateau is higher than that of the Loess Plateau and the North China Plain. This shows that the Tibet Plateau has a large temperature heating up effect, followed by the Loess Plateau. Not only does it have a higher temperature heating-up effect in the hottest month, but also has a heating-up effect on the near-surface atmosphere in the coldest plateau.Due to the influence ofheating-up effect , the Tibet Plateau is about 1.5~8°C higher than the Loess Plateau and about 6~13°C higher than the North China Plain at the same altitude .

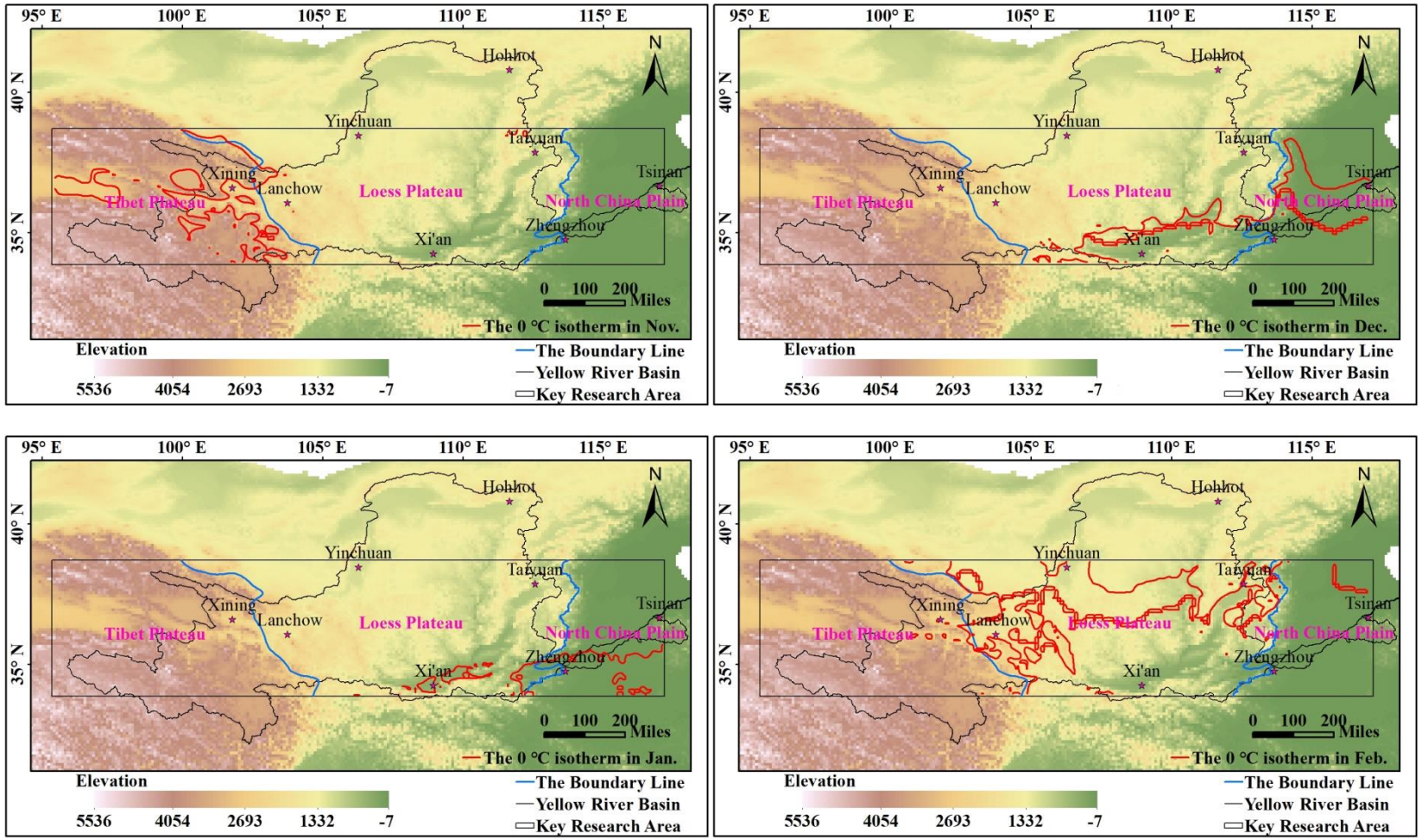
95° E
100° E
105° E
110° E
115° E
40° N
35° N
N
Hohhot
Yinchuan
Taiyuan
Xining
Lanchow
Tsinan
Zhengzhou
Xi'an
Tibet Plateau
Loess Plateau
North China Plain
0 100 200 Miles
The 0 °C isotherm in Nov.
The 0 °C isotherm in Dec.
The 0 °C isotherm in Jan.
The 0 °C isotherm in Feb.
Elevation
5536 4054 2693 1332 -7
The Boundary Line
Yellow River Basin
Key Research Area

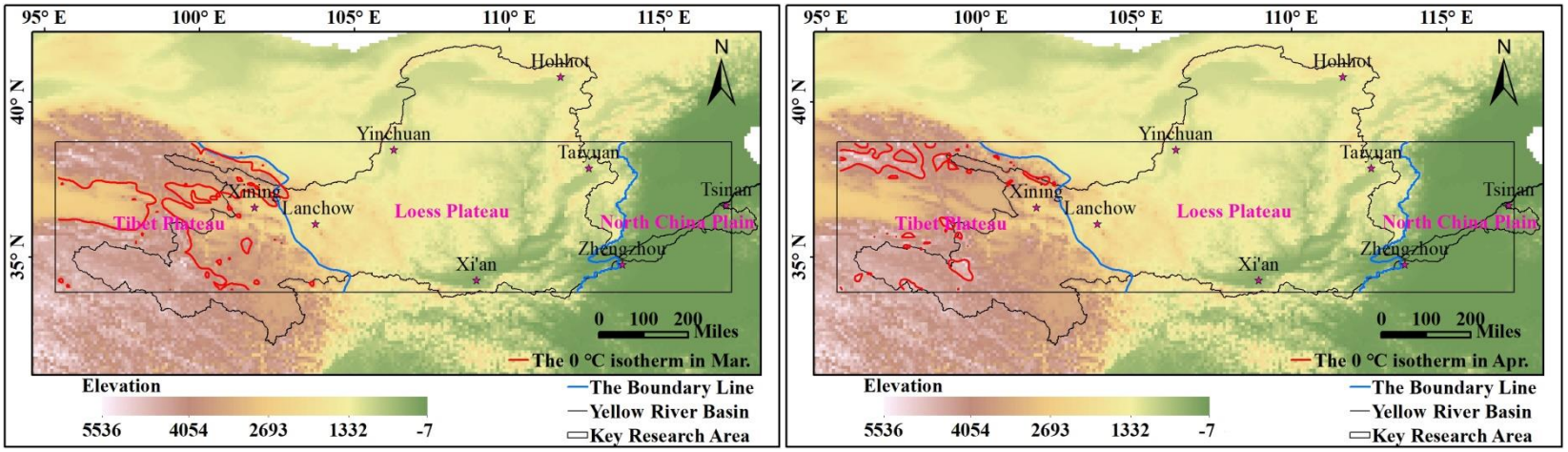

404

405 **Fig.3** Distribution pattern of 0°C isotherms in the key research area of the Yellow River Basin in the winter half year

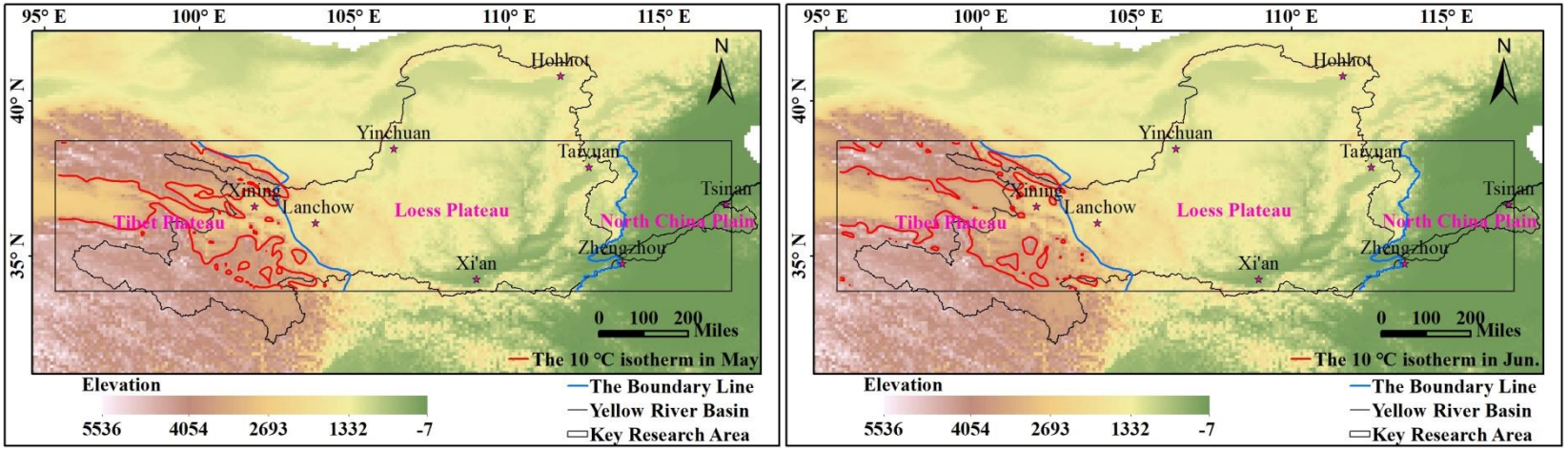

406

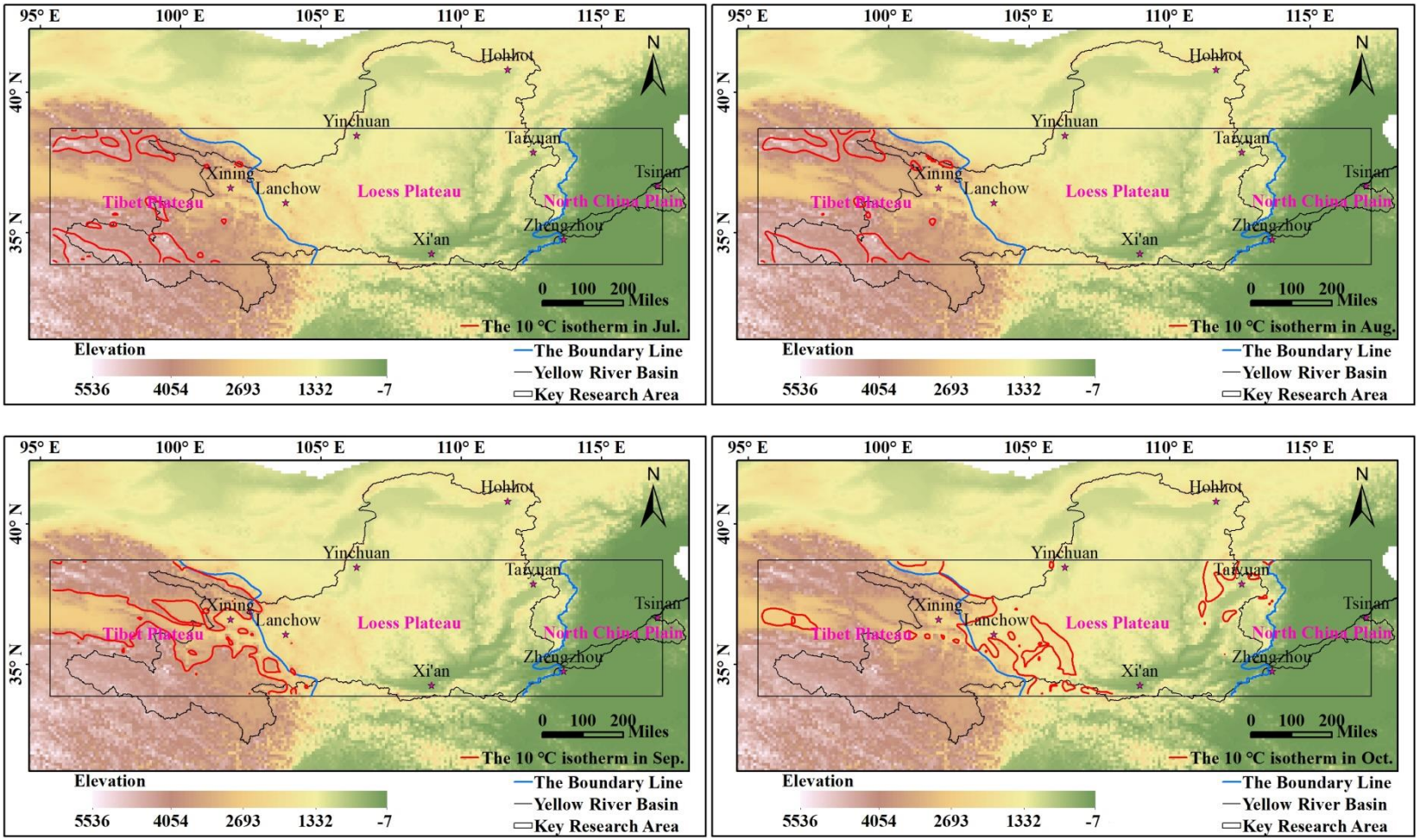

Fig.4 Distribution pattern of 10°C isotherms in the key research area of the Yellow River Basin in the summer half year

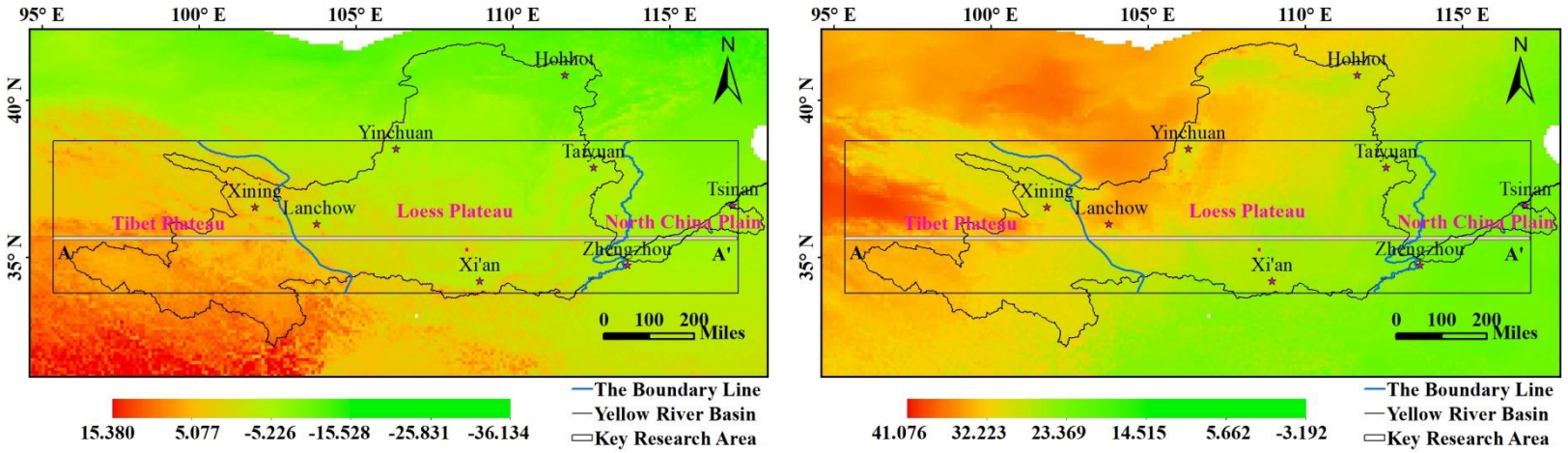

Fig. 5 Temperature distribution map of the 4500m altitude in the Yellow River Basin (left: January;right: July)

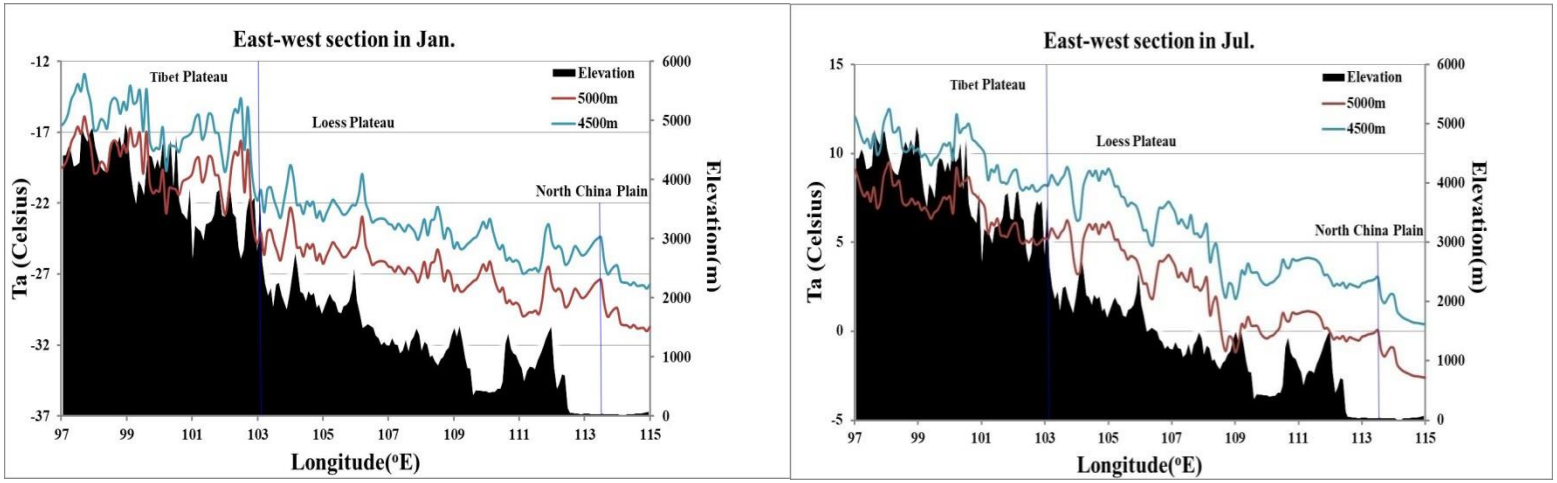

Fig. 6 Temperature profile of the plateau at 4500m and 5000m in the Yellow River Basin (AA′, left: January; right: July)

414 **Table 4**Temperature and temperature difference between the Tibet Plateau, the Loess Plateau and the North China Plain at an altitude of 4500

Area	Jan.	Feb.	Mar.	Apr.	May	Jun.	Jul.	Aug.	Sep.	Oct.	Nov.	Dec.
Tibet Plateau	-17.577	-11.265	-5.753	-2.628	4.218	6.924	9.681	9.297	4.850	-1.315	-8.964	-14.161
Loess Plateau	-24.862	-18.144	-10.632	-6.992	1.254	5.409	6.540	4.298	-0.64	-6.543	-14.498	-21.885
NorthChinaPlain	-27.882	-23.620	-16.244	-13.697	-5.403	0.591	0.757	-1.799	-5.263	-9.635	-18.621	-26.253
$\Delta T_{\text{Loess Plateau-NorthChinaPlain}}$	3.020	5.476	5.612	6.705	6.657	4.818	5.783	6.097	4.623	3.092	4.123	4.368
$\Delta T_{\text{Tibet Plateau-Loess Plateau}}$	7.285	6.879	4.879	4.364	2.964	1.515	3.141	4.999	5.490	5.228	5.534	7.724
$\Delta T_{\text{Tibet Plateau-NorthChinaPlain}}$	10.305	12.355	10.491	11.069	9.621	6.333	8.924	11.096	10.113	8.320	9.657	12.092

415

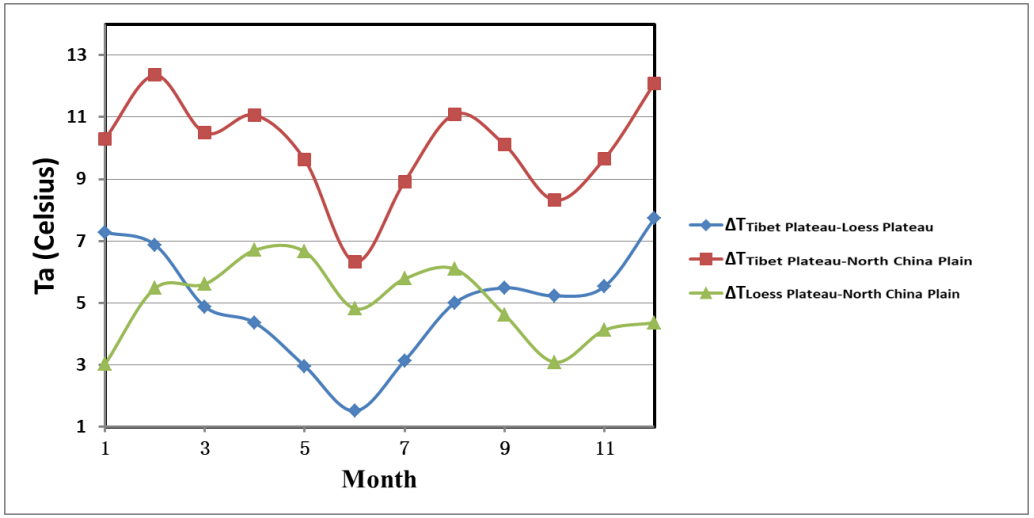

416

417 **Fig.7** Temperature difference in each month at an altitude of 4500m

4.4 Discussion

The relationship between topography and temperature is very complicated. The macroscopic influence of huge terrain can have a significant effect on the distribution and change of temperature in a wide range. The influence of local topography can also make the temperature at short distances greatly different. The annual average temperature in the Yellow River Basin is generally high in the south, low in the north, high in the east and low in the west. The areas in Henan and Shandong below Sanmenxia are the highest in the whole basin, and the upper reaches are the lowest in the whole basin. It can be seen from the annual average temperature contour map of the Yellow River Basin that the annual average temperature decreases with increasing latitude and decreases with elevation, that is, the higher the terrain, the lower the temperature. The lowest temperature in January in the basin is the lowest in January. Except for the average temperature of the individual stations in Sanmenxia to Huayuankou, the average temperature is above 0°C, and the rest of the area is below 0°C. At this time, the Mongolian high pressure is particularly strong, and the temperature distribution varies with latitude. Especially prominent, the temperature in Inner Mongolia in the upper reaches of the Yellow River is significantly lower, becoming another low-temperature zone in the basin. As a result, the temperature of the Lanzhou to Linhe section of the Yellow River is higher than that of the upstream. This is the climate of the winter in the Ningmeng section. In the lower reaches of the Yellow River, in Shandong and Shandong, although the terrain is relatively flat, the main stream is in the southwest-north-east direction, and the influence of the cold air in the southeast of the East China Sea on the coastal area is better than that in the inland. Therefore, the temperature distribution also shows the upstream and downstream. The low characteristics have formed the ridge of the downstream river section. Mainly due to the effects of the terrain and the influence of atmospheric circulation, the average temperature in January is generally low compared with other parts of the world in the same latitude. Because the Yellow River Basin is greatly affected by the East Asian winter monsoon, the whole year is the coldest in January; the temperature rises in February, and the highest temperature of the whole year in July. Later, as the summer monsoon weakened, the temperature began to decline in August. Thus, the annual variation of temperature is steep and symmetrical, with spring temperatures slightly higher than autumn.

According to the time series analysis of MODIS land surface temperature, the interannual variation of air temperature data and land surface temperature is basically similar. Due to the influence of underlying surface information or cloud and the complex topography, vegetation and climate change in the alpine valley area，there are partial RMSE between land surface temperature data and air temperature data is large. Therefore, in order to obtain mountain temperature data with higher estimation accuracy, it is necessary to further improve the inversion accuracy of MODIS land surface temperature data [46, 47], especially the extraction algorithm of MODIS land surface temperature in the alpine valley area may need further optimization and improvement [48]. In addition, the spatial resolution of MODIS land surface temperature data used in this paper is 1km. For small-scale fine mountain temperature estimation, the resolution is not high enough, and thermal infrared remote sensing data with higher spatial resolution (such as TM, OLI, etc.) can be usedfor

more detailed mountain temperature estimates.

The model of the GWR method used in this study is highly accurate. The geographically weighted regression analysis method is based on the spatial variability hypothesis model, considering the spatial variability of the relationship between variables, by estimating any given location in the study area. The regression model is built between the relevant variables and the parameters of the explanatory variables, which is very suitable for the temperature estimation in this study area. At the same time, the altitude is also introduced into the GWR estimation model as a variable, which further improves the estimation accuracy of the model. In addition, using the real-time and continuity of thermal infrared remote sensing data to estimate the temperature, it can also generate air temperature data in time series, so that the air temperature can be analyzed in time series, which helps to dynamically grasp the changes of mountain climate.

In fact, due to the influence of heating-up effect, the vertical decline rate of different regions is different. Since the vertical decline rate of temperature varies with latitude, the distance from the sea will change.In this paper, the temperature of the basin is converted to the specified altitude (4500m, 5000m) according to the vertical decreasing rate of 0.006°C/m, and the temperature difference in the basin is analyzed. This may cause uncertainty in air temperature estimation. Factors affecting temperature such as soil temperature and humidity, vegetation cover, mountain heating-up effect, slope topographic conditions, precipitation, etc., at the corresponding scale, we will obtain the corresponding detailed data in the next step to accurately estimate the heating-up effect.

5 Conclusion

(1) The time series analysis and regression analysis of MODIS surface temperature and temperature show that the temporal variation of MODIS surface temperature and temperature is similar, and the two have good correlation. Therefore, MODIS surface temperature can be used as an important factor for mountain temperature estimation. The results of geographically weighted regression analysis with MODIS surface temperature and altitude as independent variables show that the GWR method, combined with meteorological data and MODIS surface temperature, DEM, etc., can accurately estimate the temperature of the Yellow River Basin.

(2) Through the estimation of the temperature of the Yellow River Basin for 12 months, the variation of temperature and time in the study area was obtained. According to the spatial distribution of the estimated air temperature, the temperature in each month is generally low in the west and high in the east, followed by the north-central characteristics, and the reason is that the west is located in high altitude areas such as plateaus and mountains, and the annual temperature is low. The central and northern parts are mainly the central Long, the eastern Long of Loess Plateau and the Inner Mongolia Plateau and it has a deep inland rainfall and a dry climate; the downstream is located in the plain area and has a low latitude, and the annual temperature is high, so the temperature is high. It can be seen that the temperature range in January (the coldest month) is -20.612~6.499°C, and the temperature range in July (the hottest month) is 0.906~35.704°C. The Yellow River Basin has aobvioustemperature heating-up effect, and the isotherm altitude changes can also be seen that the Yellow River Basin has gradually increased from the east to the west. The

temperature of the Tibet Plateau is higher than that of the Loess Plateau and the North China Plain, and the highest temperature appears in the western part of the plateau. At the same altitude, the Tibet Plateau is about 1.5~8°C higher than the Loess Plateau and about 6~13°C higher than the North China Plain. In summary, the use of meteorological data and corresponding MODIS surface temperature data, regression analysis of DEM data and weather station data verification results show that this type of data can be used to estimate the temperature of the Yellow River Basin fairly accurately and to study the difference in temperature increase effect in the region, which lays a foundation for revealing the plateau ecological effect quantitatively .

Although the focus of this paper is on the estimation of the mean value, the method proposed in this paper can also be applied to determine the daily maximum, minimum and average temperature. In addition, more variables (such as NDVI, precipitation, albedo, etc.) will be considered in the future to explore whether they improve the accuracy of model estimation.

Acknowledgments: The research work was financially supported by the National Science & Technology Infrastructure of China (No. 2005DKA32300), the Major Projects of the Ministry of Education (No. 16JJD770019), the Data Sharing Infrastructure of Earth System Science Data Centre of the Lower Yellow River Region (http://henu.geodata.cn).

Funding: This research was funded jointly by the National Science and Technology Platform Construction Project of China (2005DKA32300) and Major Projects of the Ministry of Education Base (16JJD770019) in China, the Data Sharing Infrastructure of Earth System Science Data Centre of the Lower Yellow River Region (http://henu.geodata.cn).

Author Contributions: All authors conceived, designed, and implemented the study. Conceptualization: Z.P.; methodology: F.Q.; software: F.Q., Z.P.; validation: J.Z. and F.Q.; formal analysis: F.Q.J.Z.; investigation and resources: J.Z.; data curation: J.Z; original draft preparation: Z.P., F.Q.;and review and editing: F.Q..

Conflicts of Interest: The authors declare no conflicts of interest.

References

1. Barry R G. Mountain Weather and Climate. London and New York: Routledge, 1992.
2. Barry R G. Mountain Weather and Climate. Boulder, USA: University of Colorado, 2008.
3. Flenley J. Ultraviolet insulation and the tropical rainforest: Altitudinal variations, Quaternary and recent change,extinctions, and biodiversity//Tropical Rainforest Responses to Climatic Change. Springer, 2007: 219-235.
4. Holtmeier F.-K. Mountain timberlines: Ecology, patchiness, and dynamics//Advances in Global Change Research. Boston:Kluwer Academic Publishers, 2003.
5. Wang Yuenan, Zhang Bo, Chen Longxun et al. Relationship between the atmospheric heat source over Tibetan Plateau andthe heat source and general circulation over East Asia. Chinese Science Bulletin, 2008, 53(21): 3387-3394.
6. Ukraintseva, V.V. *Mountain Weather and Climate*; Cambridge University Press: 2008; 10.1029/EO063i051p01225pp. 919-927.
7. Ren, G.Y.; Ming-Zhi, X.U.; Chu, Z.Y.; Guo, J.; Qing-Xiang, L.I.; Liu, X.N. Changes of Surface Air Temperature in China During 1951—2004. *Climatic Environmental Research* **2005**, *10*, 717-727.
8. Shi, Y.; Jiang, Z.; Dong, L.; Shen, S. Statistical Estimation of High-resolution Surface Air Temperature from MODIS over the Yangtze River Delta, China. *Journal of Meteorological*

Research **2017**, *31*, 448-454, doi:10.1007/s13351-017-6073-y.
9. Noi Phan, T.; Kappas, M.; Degener, J. Different combination of MODIS land surface temperature data for daily air surface temperature estimation in North West Vietnam. In Proceedings of EGU General Assembly Conference.
10. Liu, S.; Su, H.; Tian, J.; Zhang, R.; Wang, W.; Wu, Y. Evaluating Four Remote Sensing Methods for Estimating Surface Air Temperature on a Regional Scale. *Journal of Applied Meteorology Climatology* **2017**, *56*, 803-814, doi:10.1175/JAMC-D-16-0188.1.
11. Pan, P.; Yali, Z.; Jijun, W. Spatial−temporal Variations of Temperature and the Cause Analyese in the Yellow River Valley during Recent 50 years. *Climatic and Environmental Research (in Chinese)* **2014**, *19*, 477−485.
12. Huang, X.; Ma, L.; Liu, T.X.; Wang, J.R.; Liu, D.H.; Li, H.Y. Temperature mutation and globe warming stagnate study in typical area of Yellow River basin in recently 60 years. *China Environmental Science* **2016**, *36*, 3253-3262
13. Janatian, N.; Sadeghi, M.; Sanaeinejad, S.H.; Bakhshian, E.; Farid, A.; Hasheminia, S.M.; Ghazanfari, S. A Statistical Framework for Estimating Air Temperature using MODIS Land Surface Temperature Data. *International Journal of Climatology* **2017**, *37*, doi:10.1002/joc.4766.
14. Hongmei, Z. Estimation of Daily Average Near-surface Air Temperature Using MODIS and AIRS Data. In Proceedings of International Conference on Frontiers of Sensors Technologies 2017, Shenzhen, China.
15. Han, Y.; Weiqiang, M.A.; Wang, B.; Yaoming, M.A.; Tian, R. Climatic Characteristics of Rainfall Change over the Qinghai-Tibetan Plateau from 1980 to 2013. *Plateau Meteorology* **2017**, *06*, 1477-1486.
16. Hooker, J.; Duveiller, G.; Cescatti, A. A Global Dataset of Air Temperature Derived from Satellite Remote Sensing and Weather Stations. *Sci Data* **2018**, *5*, 180246, doi:10.1038/sdata.2018.246.
17. Wen, J.Y.; Yang, J. Relationship Analysis between Road Temperature and Air Temperature by Using Method of Moments Estimation. *Northern Communications* **2016**, *4*, 111-117, doi:10.15996 /j.cnki.bfjt.2016.04.028.
18. Sterin, A.M.; Timofeev, A.A. Estimation of Surface Air Temperature Trends over the Russian Federation Territory using the Quantile Regression Method. *Russian Meteorology Hydrology* **2016**, *41*, 388-397, doi:10.3103/S1068373916060029.
19. Yonghui, Y.; Baiping, Z.; Fang, H. MODIS-based Air Temperature Estimation in the Hengduan Mountains and Its Spatio-temporal Analysis. *Acta Geographica Sinica* **2011**, *66*, 917-927, doi:10.4028/www.scientific.net/AMR.102-104.17.
20. Hwang, J.; Choi, Y.S.; Kim, W.M.; Su, H.; Jiang, J.H. Observational Estimation of Radiative Feedback to Surface Air Temperature over Northern High Latitudes. *Climate Dynamics* **2016**, *50*, 1-14, doi:10.1007/s00382-017-3629-6.
21. Xiaoxiao, J.I.; Liu, C.; Pan, J.; Liang, J.; Tong, J.; Feng, Q.; Yinlong, X.U. Surface Air Temperature Change over China Based on the PRECIS_QUMP Ensemble Simulation. *Climatic Environmental Research* **2015**, *20*, 500−510, doi:10.3878/j.issn.1006-9585.2015.14185.
22. Chen, F.; Liu, Y.; Liu, Q.; Qin, F. A Statistical Method Based on Remote Sensing for the Estimation of Air Temperature in China. *International Journal of Climatology* **2015**, *35*, 2131-2143, doi:10.1002/joc.4113.
23. Sun, H.; Chen, Y.; Gong, A.; Zhao, X.; Zhan, W.; Wang, M. Estimating Mean Air Temperature

using MODIS Day and Night Land Surface Temperatures. *Theoretical Applied Climatology* **2014**, *118*, 81-92, doi:10.1007/s00704-013-1033-7.
24. Perevedentsev, Y.P.; Shantalinskii, K.M. Estimation of Contemporary Observed Variations of Air Temperature and Wind Speed in the Troposphere of the Northern Hemisphere. *Russian Meteorology Hydrology* **2014**, *39*, 650-659, doi:10.3103/S1068373914100021.
25. Fu, G.; Shen, Z.; Zhang, X.; Shi, P.; Zhang, Y.; Wu, J. Estimating Air Temperature of an Alpine Meadow on the Northern Tibetan Plateau using MODIS Land Surface Temperature. *Acta Ecologica Sinica* **2011**, *31*, 8-13, doi:10.1016/j.chnaes.2010.11.002.
26. Han, F.; Zhang, B.; Xican, L.I.; Liang, Y.; Tan, J.; Zhang, S. MODIS-based Estimation of Mass Elevation Effect in the Tibetan Plateau and Its Ecological Effect. *Mountain Research* **2016**, *34*, 788-798, doi:10.16089/j.cnki.1008-2786.000187.
27. Han, F.; Zhang, B.P.; Zhao, F.; Guo, B.; Liang, T. Estimation of Mass Elevation Effect and Its Annual Variation Based on MODIS and NECP Data in the Tibetan Plateau. *Journal of Mountain Science* **2018**, *15*, 1510-1519, doi:10.1007/s11629-018-4865-x.
28. Didari; Shohreh; Norouzi; Hamidreza; Zand-Parsa; Shahrokh; Khanbilvardi; Reza. Estimation of Daily Minimum Land Surface Air Temperature Using MODIS Data in Southern Iran. *Theoretical Applied Climatology* **2016**, *130*, 1-13, doi:10.1007/s00704-016-1945-0.
29. Zhang, F., Zhang, H, Ye, M. Air Temperature Estimation Using MODIS LST Data Based on Ground Measurements on the Glaciers in the Tibetan Plateau. In Proceedings of AGU Fall Meeting 2017.
30. Cai, Y.; Chen, G.; Wang, Y.; Yang, L. Impacts of Land Cover and Seasonal Variation on Maximum Air Temperature Estimation Using MODIS Imagery. *Remote Sens.* **2017**, *9*, doi:10.20944/preprints201703.0021.v1.
31. Tang, B.-H.; Zhan, C.; Li, Z.-L.; Wu, H.; Tang, R. Estimation of Land Surface Temperature From MODIS Data for the Atmosphere With Air Temperature Inversion Profile. *IEEE Journal of Selected Topics in Applied Earth Observations and Remote Sensing* **2017**, *10*, 2976-2983, doi:10.1109/jstars.2016.2634629.
32. Yonghui, Y.; Baiping, Z. MODIS-based Estimation of Air Temperature of the Tibetan Plateau. *Journal of Geographical Sciences* **2013**, *23*, 627-640, doi:10.1007/s11442-013-1033-7.
33. Bustos, E.; Meza, F.J. A method to estimate maximum and minimum air temperature using MODIS surface temperature and vegetation data: application to the Maipo Basin, Chile. *Theoretical and Applied Climatology* **2014**, *120*, 211-226, doi:10.1007/s00704-014-1167-2.
34. Kisi, O.; Ay, M. Comparison of Mann–Kendall and Innovative Trend Method for Water Quality Parameters of the Kizilirmak River, Turkey. *Journal of Hydrology* **2014**, *513*, 362-375, doi:10.1016/j.jhydrol.2014.03.005.
35. Jianwei, X.U.; Gao, Y. Validation of Summer Surface Air Temperature and Precipitation Simulation over Heihe River Basin. *Plateau Meteorology* **2014**, *18*, 42-50.
36. Chen, J.L.; Li, G.S. Retraction statement: Estimation of monthly mean solar radiation from air temperature in combination with other routinely observed meteorological data in Yangtze River Basin in China. *Meteorological Applications* **2014**, *21*, 459-459.
37. Gundalia, M.J. Estimation of Pan Evaporation Using Mean Air Temperature and Radiation for Monsoon Season in Junagadh Region. *International Journal of Engineering Research* **2013**, *3*, pp.64-70.
38. Alvares; Alcarde, C.; Goncalves, D.M.; Leonardo, J.; Stape. Modeling Monthly Mean Air

Temperature for Brazil. *Theoretical Applied Climatology* **2013**, *113*, 407-427, doi:10.1007/s00704-012-0796-6.
39. Sheffield, J.; Wood, E.F.; Roderick, M.L. Little Change in Global Drought over the Past 60 years. *Nature* **2012**, *491*, 435-438, doi:10.1038/nature11575.
40. Río, S.D.; Herrero, L.; Penas, A. Recent trends in Mean Maximum and Minimum Air Temperatures over Spain (1961–2006). *Theoretical Applied Climatology* **2012**, *109*, 605-626, doi:10.1007/s00704-012-0593-2.
41. Verbesselt J,Hyndman R,Zeileis A,et al.Phenological change detection while accounting for abrupt and gradual trends in satellite image time series [J]. Remote Sensing of Environment，2010,114(12) : 2970- 2980.
42. Jobbagy, E.G.; Jackson, R.B. Global Controls of Forest Line Elevation in the Northern and Southern Hemispheres. *Global Ecology Biogeography* **2010**, *9*, 253-268, doi:10.1046/j.1365-2699.2000.00162.x.
43. Shen, S.; Leptoukh, G.G. Estimation of Surface Air Temperature over Central and Eastern Eurasia from MODIS Land Surface Temperature. *Environmental Research Letters* **2011**, *6*, 045206, doi:10.1088/1748-9326/6/4/045206.
44. Gouvas, M.A.; Sakellariou, N.K.; Kambezidis, H.D. Estimation of the Monthly and Annual Mean Maximum and Mean Minimum Air Temperature Values in Greece. *Meteorology Atmospheric Physics* **2011**, *110*, 143-149, doi:10.1007/s00703-010-0111-y.
45. Ren, Y.; Zhang, X.Q.; Peng, L.L. Construction and Analysis of Mean Air Temperature Anomaly Series for the Qinghai-Xizang Plateau during 1951-2006. *Plateau Meteorology* **2010**, *29*, 572-578, doi:10.3788/gzxb20103906.0998.
46. Boban, A.; Lambert, C.; Hermans, C. Application of the Land Surface Temperature from MODIS in the Estimation of Gross Primary Productivity for a Subtropical Pinus Plantation in Southern China. In Proceedings of International Conference on Remote Sensing, Environment and Transportation Engineering; pp. 337-346.
47. Shen, S.; Leptoukh, G.G.; Gerasimov, I.V. Estimation of Surface Air Temperature from MODIS High Resolution Land Surface Temperature over Northern China. In Proceedings of Fall Meeting 2010.
48. Yoo, C.; Im, J.; Park, S.; Quackenbush, L.J. Estimation of Daily Maximum and Minimum Air Temperatures in Urban Landscapes using MODIS Time Series Satellite Data. *ISPRS Journal of Photogrammetry and Remote Sensing* **2018**, *137*, 149-162, doi:10.1016/j.isprsjprs.2018.01.018.

Figures

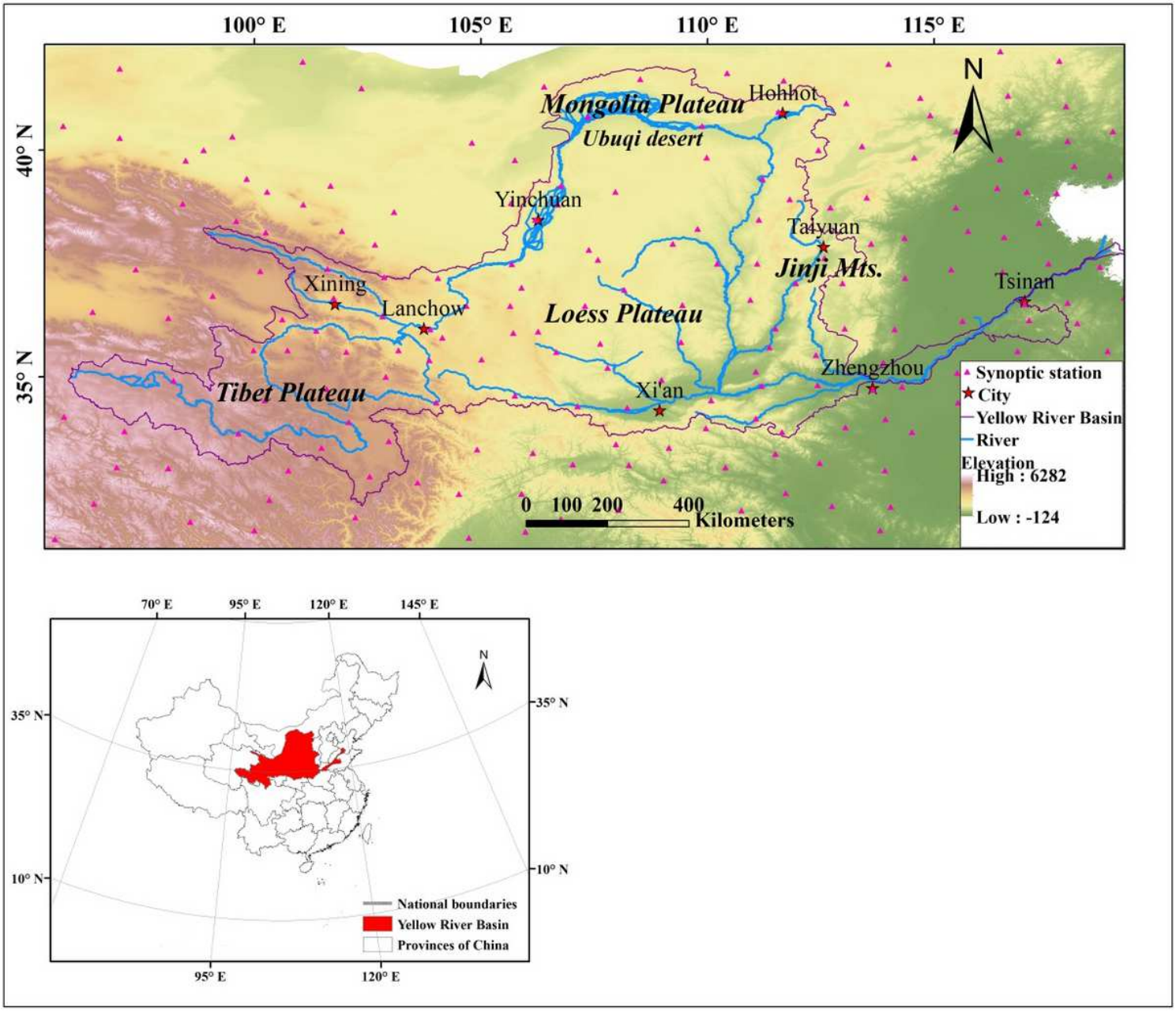

Figure 1

Study area and weather station distribution map. Note: The designations employed and the presentation of the material on this map do not imply the expression of any opinion whatsoever on the part of Research Square concerning the legal status of any country, territory, city or area or of its authorities, or concerning the delimitation of its frontiers or boundaries. This map has been provided by the authors.

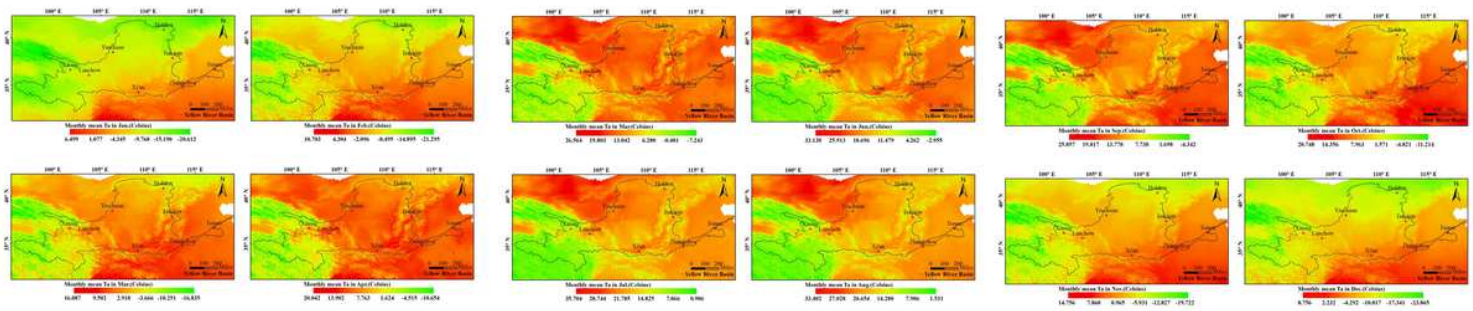

Figure 2

Spatial distribution of monthly mean Ta in the study area. Note: The designations employed and the presentation of the material on this map do not imply the expression of any opinion whatsoever on the part of Research Square concerning the legal status of any country, territory, city or area or of its authorities, or concerning the delimitation of its frontiers or boundaries. This map has been provided by the authors.

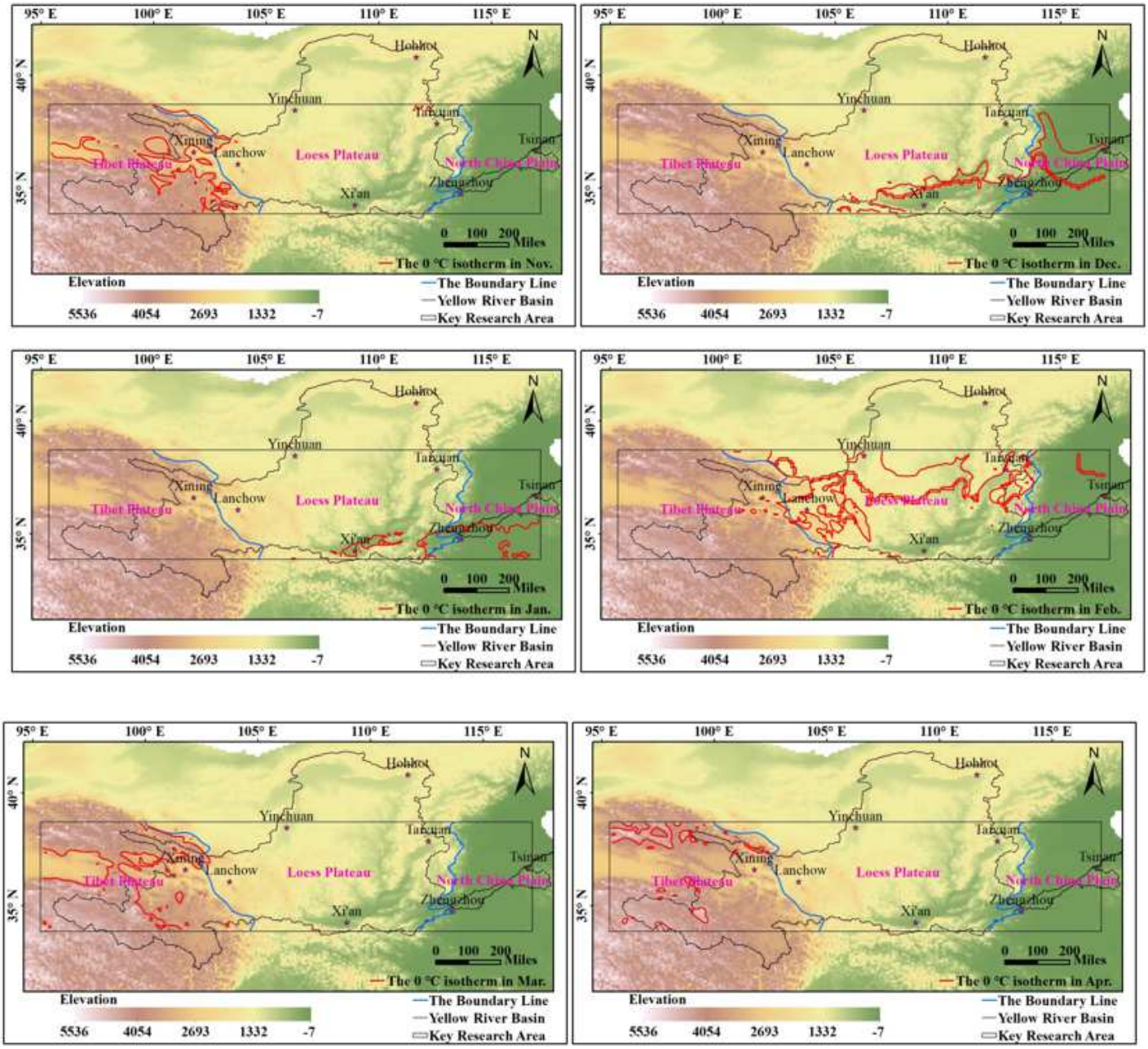

Figure 3

Distribution pattern of 0°C isotherms in the key research area of the Yellow River Basin in the winter half year. Note: The designations employed and the presentation of the material on this map do not imply the expression of any opinion whatsoever on the part of Research Square concerning the legal status of any country, territory, city or area or of its authorities, or concerning the delimitation of its frontiers or boundaries. This map has been provided by the authors.

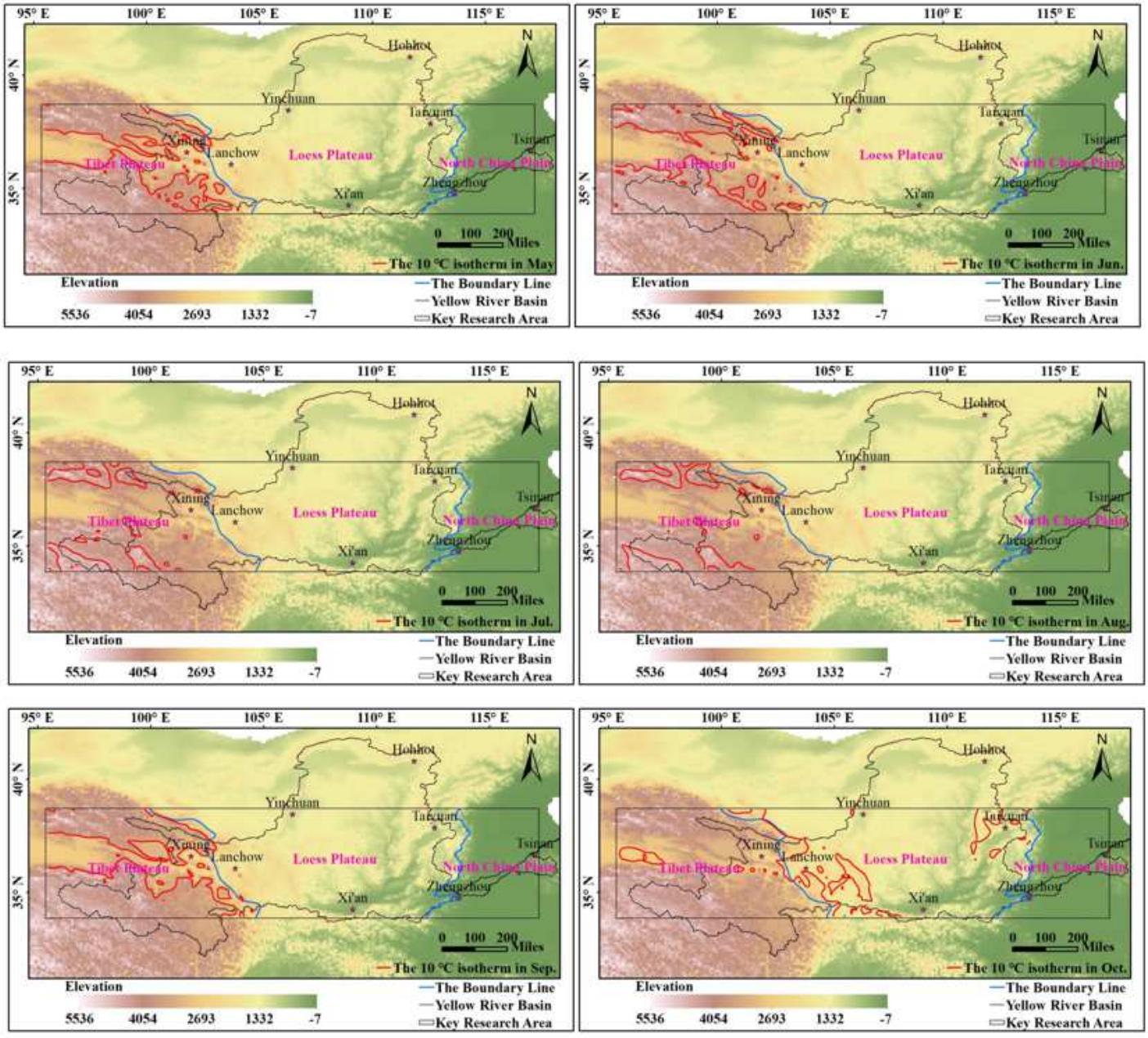

Figure 4

Distribution pattern of 10°C isotherms in the key research area of the Yellow River Basin in the summer half year. Note: The designations employed and the presentation of the material on this map do not imply the expression of any opinion whatsoever on the part of Research Square concerning the legal status of any country, territory, city or area or of its authorities, or concerning the delimitation of its frontiers or boundaries. This map has been provided by the authors.

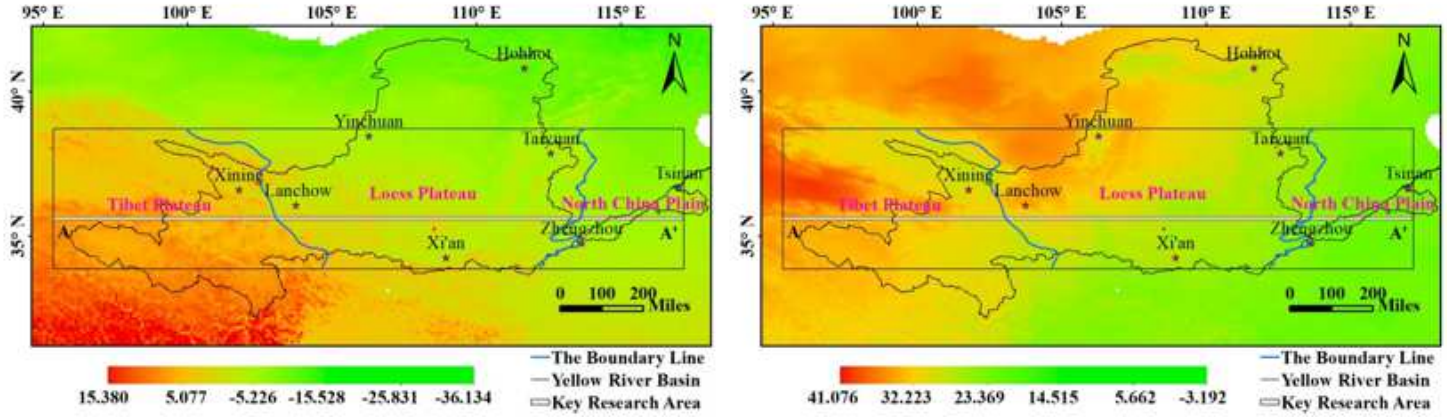

Figure 5

Temperature distribution map of the 4500m altitude in the Yellow River Basin (left: January;right: July). Note: The designations employed and the presentation of the material on this map do not imply the expression of any opinion whatsoever on the part of Research Square concerning the legal status of any country, territory, city or area or of its authorities, or concerning the delimitation of its frontiers or boundaries. This map has been provided by the authors.

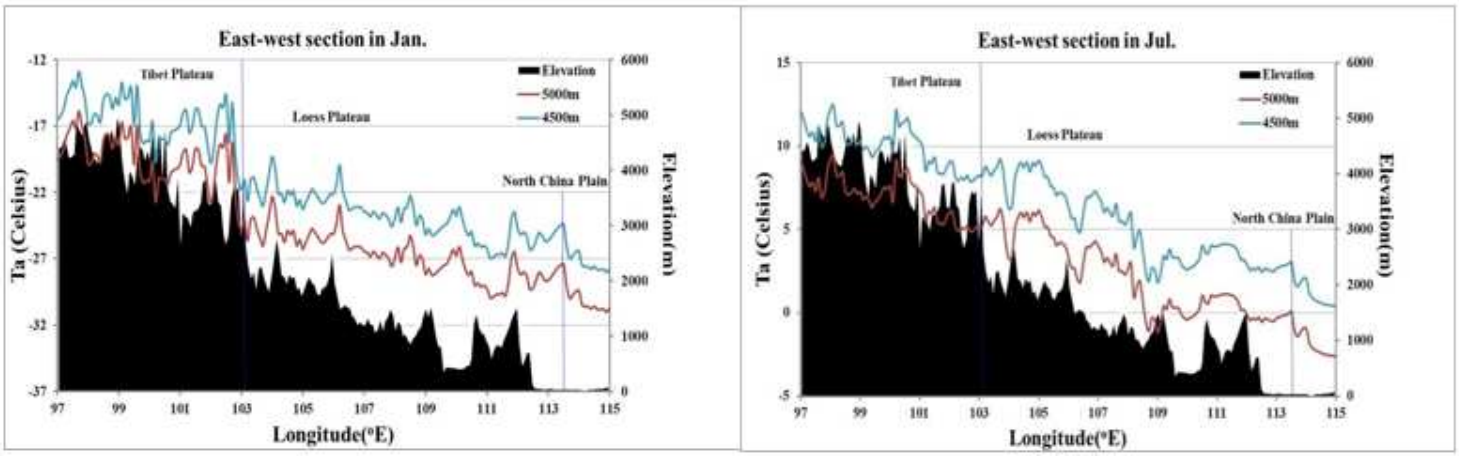

Figure 6

Temperature profile of the plateau at 4500m and 5000m in the Yellow River Basin (AA', left: January; right: July)

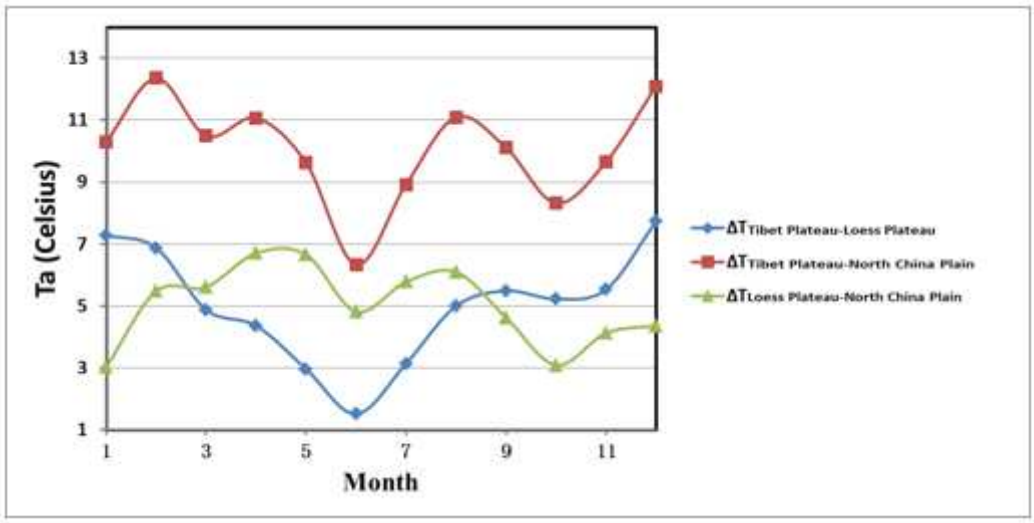

Figure 7

Temperature difference in each month at an altitude of 4500m